

Review

Covalent Organic Frameworks for Chemical and Biological Sensing

Shiji Zhang¹, Danqing Liu^{1,*} and Guangtong Wang^{2,*} 

¹ School of Material Science and Chemical Engineering, Harbin University of Science and Technology, Harbin 150080, China; zhangcentury975@gmail.com

² Key Laboratory of Micro-Systems and Micro-Structures Manufacturing, Ministry of Education, Harbin Institute of Technology, Harbin 150080, China

* Correspondence: danqingliu76@163.com (D.L.); wgt@hit.edu.cn (G.W.)

Abstract: Covalent organic frameworks (COFs) are a class of crystalline porous organic polymers with polygonal porosity and highly ordered structures. The most prominent feature of the COFs is their excellent crystallinity and highly ordered modifiable one-dimensional pores. Since the first report of them in 2005, COFs with various structures were successfully synthesized and their applications in a wide range of fields including gas storage, pollution removal, catalysis, and optoelectronics explored. In the meantime, COFs also exhibited good performance in chemical and biological sensing, because their highly ordered modifiable pores allowed the selective adsorption of the analytes, and the interaction between the analytes and the COFs' skeletons may lead to a detectable change in the optical or electrical properties of the COFs. In this review, we firstly demonstrate the basic principles of COFs-based chemical and biological sensing, then briefly summarize the applications of COFs in sensing some substances of practical value, including some gases, ions, organic compounds, and biomolecules. Finally, we discuss the trends and the challenges of COFs-based chemical and biological sensing.

Keywords: covalent organic frameworks; porous material; sensor; gas; humidity; ions; explosives; drug; biosensing



Citation: Zhang, S.; Liu, D.; Wang, G. Covalent Organic Frameworks for Chemical and Biological Sensing. *Molecules* **2022**, *27*, 2586. <https://doi.org/10.3390/molecules27082586>

Academic Editors: Ye Yuan and Yajie Yang

Received: 22 February 2022

Accepted: 1 April 2022

Published: 18 April 2022

Publisher's Note: MDPI stays neutral with regard to jurisdictional claims in published maps and institutional affiliations.



Copyright: © 2022 by the authors. Licensee MDPI, Basel, Switzerland. This article is an open access article distributed under the terms and conditions of the Creative Commons Attribution (CC BY) license (<https://creativecommons.org/licenses/by/4.0/>).

1. Introduction

Detecting chemicals or biomolecules is one of the essential goals of analytical chemistry and plays an important role in a wide range of fields including environmental protection, clinic diagnosis, health monitoring, public security, food industry, et al. Thanks to the fast development of instrument science and material science in recent decades, instruments for detecting diverse analytes have been developed. Nowadays, various spectrophotometers, chromatographs, and electrochemical analyzers can be found as conventional analytical equipment in laboratories, factories, and even hospitals. A large number of chemicals and biomolecules can be detected with satisfactory accuracy. However, due to the growing concern for environmental security and healthcare, the demand for fast, real-time, and portable analytical instruments has been increasing. In recent years, plenty of efforts have been devoted to developing portable, wearable, or even implantable sensors for detecting impurities, pollutants, drugs, and physiological indexes [1–7].

In principle, two key concerns should be carefully considered for detecting a particular analyte. One is to selectively recognize and separate the analyte from the samples. Although some analytes with special physical properties can be separated by simple methods such as filtration, centrifugation, evaporation, et al., most analytes' separation so far relies on molecular recognition and selective adsorption based on physical, chemical, or biological interaction. Therefore, it is crucial to design and prepare a sort of material that can selectively interact and capture the analyte from the samples during the development of a chemical or biological sensor. Until now, 2D materials such as graphene [8,9], BN [10],

MoS₂ [11], WS₂ [12], and MXene [13], and porous materials including zeolites [14], metal organic frameworks (MOFs) [15–17], and covalent organic frameworks (COFs) [18–20] were usually chosen as the candidates for selective analytes' capture. A number of chemical or biological sensors based on the above materials have been constructed. The other key concern for chemical and biological sensing is converting the uptake of the analyte to a detectable signal. The signal can be optical, electrical, thermal, or acoustic. In practice, electrical and optical signals were usually applied since they can be real-time and quantitatively monitored.

COFs are a class of crystalline porous organic polymers with polygonal porosity and highly ordered structures [21–23]. As shown in Figure 1, the porosity of the COFs originated from their unique structural design of monomers. In general, the monomers for synthesizing COFs can be roughly divided into two categories. One is the star-like multi-functional monomer that acts as the “knot” in the framework and the other is the linear double functional monomer that can be used as the “edge”. The knots and edges are usually linked by dynamic covalent bonds such as imine, borate ester, hydrazone, carbon-carbon double bond, et al. (Table 1). The dynamic nature of these linkages allows the formation of highly regular, repeated structures with ordered polygonal pores of which the sizes and shapes are determined by the molecular structures of the “knot” and “edge” molecules [19,21,24,25]. Furthermore, functional substituents can be easily introduced to the pore of the COFs by pre-linking it onto the “knots” or “edges” before the synthesis of the COFs or by immobilizing it onto the wall of the pore after the formation of the COFs. In addition, the pores and functional groups on the COFs' skeletons allows further modification of the COFs by loading nanoparticles or immobilizing nucleic acid or enzymes into their pores or onto their 2D sheets [26–29]. Thus, it seems that there are infinite possibilities for creating new functional COFs or COF-based hybrid materials. Since the first report by Yaghi et al., in 2005 [30], numerous COFs with various structures and functions have been presented. The application of COFs has been extended to the fields of energy storage and conversion [31,32], optoelectronics [33], gas adsorption and separation [31,34–36], sensing [18–20], catalysis [37–41], pollutant removal [42,43], battery [44], drug release [45], and so on.

COFs nowadays have been proved to be an ideal platform for chemical and biological sensing. The ordered pore structure of COFs benefits the selective adsorption of the analytes. More importantly, by the pre-design of the monomers, binding sites that can specifically interact with the analyte can be introduced into the “knots” or “edges” of the COFs to further enhance the selectivity of the analytes' adsorption. Therefore, COFs have exhibited a great advantage in the selective capture and enrichment of the analyte. Furthermore, the analyte adsorption may also affect the optical, electrical, or catalytic properties of the COFs, resulting in a detectable change of color, fluorescence, conductivity, capacitance, or (photo) electrochemical currents, et al. [18]. It can be found that the two key problems of fabricating a chemical or biological sensor are possibly simultaneously solved by one well-designed COF or COF-based hybrid material. Therefore, plenty of chemical or biological sensors on the basis of COFs or COFs-based hybrids have been reported in recent years [18–22,46].

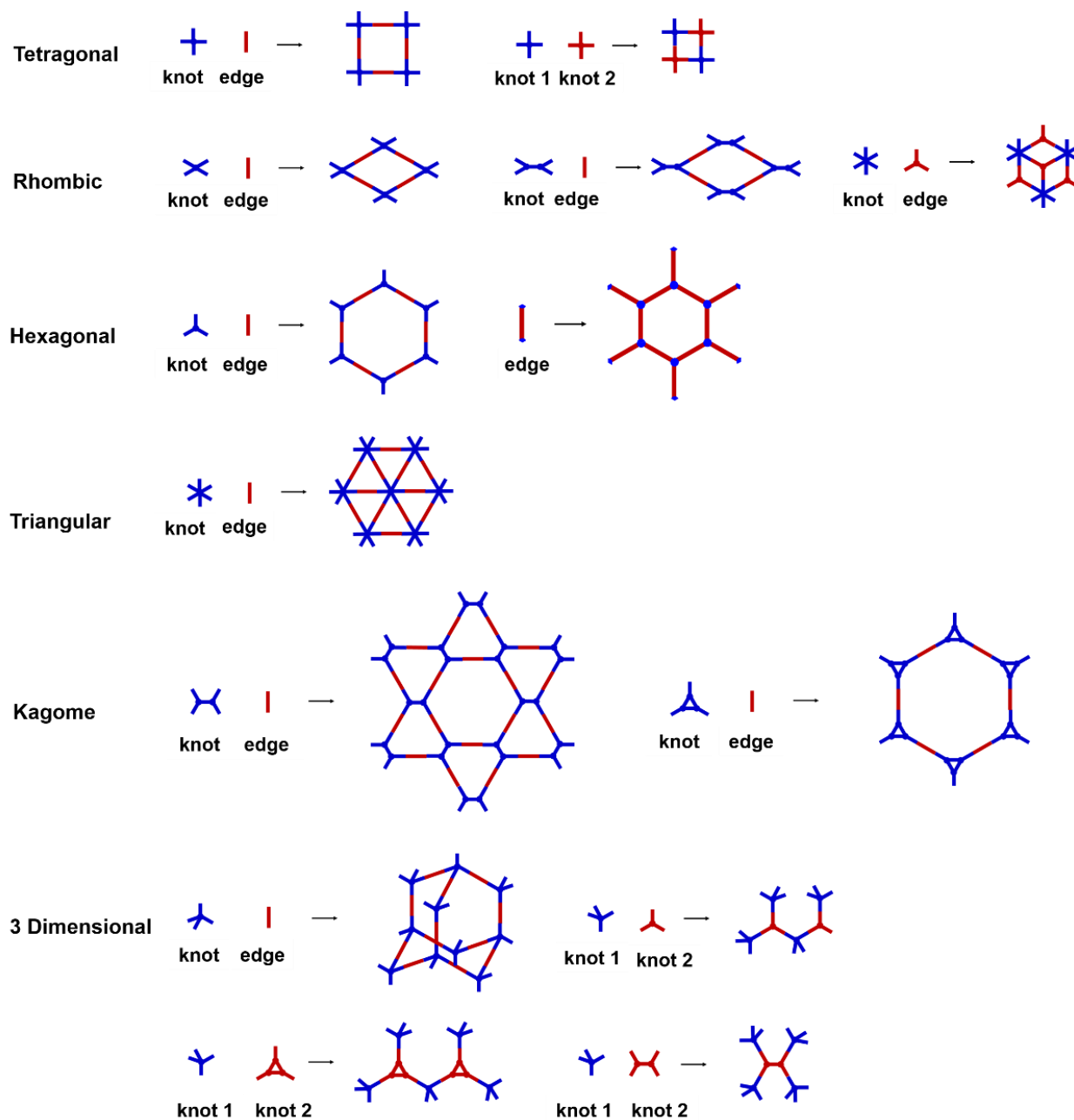


Figure 1. The basic topology of the COFs.

In this review, we firstly discuss the basic principles to design a COF that can selectively adsorb the analyte, then demonstrate the detectable signals that are probably generated by COFs resulting from the analyte adsorption. Successively, we briefly summarize the application of COFs in detecting some substances of practical value, including some gases, ions, organic compounds, and biomolecules. Finally, we discuss the main challenges and future perspectives of COFs-based chemical or biological sensors.

Table 1. The dynamic linkages for COF synthesis.

| Name | Monomer 1 | Monomer 2 | Linker |
|-----------------|-----------|-----------|--------|
| Boronate | | | |
| Imine | $--NH_2$ | | |
| Hydrazone | | | |
| Maleimide | $--NH_2$ | | |
| Phenazine | | | |
| Acrylonitrile | | | |
| Triazine | | | |
| Borazine | | | |
| Benzimidazole | | | |
| Benzobisoxazole | | | |

2. Basic Principles of COF-Based Sensing

In recent years, COF-based chemical or biological sensors on the basis of various mechanisms were presented. Although there are still a few exceptions, some principles, strategies, and experiences for fabricating a COF-based sensor can be summarized from the numerous reports. In this section, we will firstly discuss the basic principles for designing

a COF that can enrich the analyte. Then we demonstrate some detectable signals that can be produced by the adsorption of the analyte.

2.1. Designing a COF or COF-Based Hybrid Material for Selective Adsorption

The porous structure of the COF results in its extraordinary adsorption capacity. However, compared with other types of porous materials, the predominant characteristic of COFs is the designability of the pores. Inspired by the recognition between the enzyme and its substrate, the key points to design a COF that can enrich the analyte are creating a suitable space allowing the load of the analyte and introducing binding sites to selectively interact with the analyte. Hence, the shape and size of the COF pores should be firstly considered. In general, the shape of the pores is mainly determined by the topology of the “knot” monomer (Figure 1). For example, to obtain a hexagonal pore, three-armed planar rigid “knot” monomers, such as the derivatives of triazine, triphenyl benzene, triphenylene derivatives, et al. were usually applied. In addition, four-armed planar rigid “knot” monomers were often used for fabricating a tetragonal pore, while the size of the COF pores depends on the length of both the “edge” monomer and the arms of the “knot” monomers. As shown in Figure 2, it can be easily enlarged by choosing a longer “edge” monomer or a “knot” molecule with longer arms. Thus, it can be found that both the shape and size of the COFs pores can be pre-designed by choosing the “knot” and “edge” monomers [21,24]. To effectively adsorb the analyte, the pore shape and size should be carefully designed to at least allow the analyte molecule to enter. Furthermore, for discriminating the interferences of a similar molecular shape and size, in general, a binding site is needed that can selectively interact with the analyte. The binding site can be the innate groups on the COF skeleton. For example, as shown in Figure 3a, the imine linkage is pH sensitive. It is a good binding site for capturing H^+ in the solution or the acid gases like HCl and Trifluoroacetic acid (TFA) [47,48]. However, in other cases, as shown in Figure 3b, the binding site is pre-linked onto one of the monomers before the synthesis of the COFs. For example, thiol or thioether groups are able to selectively adsorb the heavy metal ions like Hg^{2+} . Thus, thioether was covalently pre-linked onto the “edge” monomer, yielding a thioether-containing COF (COF-LZU8) [42]. It was shown that COF-LZU8 performed well in selectively capturing and detecting Hg^{2+} . In addition, the binding site can be also introduced after the formation of COFs, which is also called “post-functionalization” of COFs. For instance, Au nanoparticles (AuNPs) can form an amalgam layer with Hg^{2+} under the reduction of citric acid (Figure 3c). Hence, to efficiently capture and detect the trace amount of Hg^{2+} , AuNPs were doped on the nanosheet of a bipyridine-containing COF by the in situ growth method to form a COF-based hybrid material. It was found that the huge specific surface area of the COF-AuNPs hybrid material can significantly enhance the sensitivity of the Hg^{2+} detection [29]. Moreover, except for in situ growth, the binding site can be also externally introduced onto the 2D sheet of the COFs. For example, as shown in Figure 3d, to selectively detect enrofloxacin, a kind of antibiotic, an enrofloxacin-targeted aptamer was immobilized onto a 2D sheet of COF via π - π stacking and electrostatic interaction to yield an aptamer-functionalized COF hybrid [49]. Then the hybrid was coated onto a gold electrode. It can selectively capture the enrofloxacin in the sample solution and result in a detectable change in the electrode conductivity.

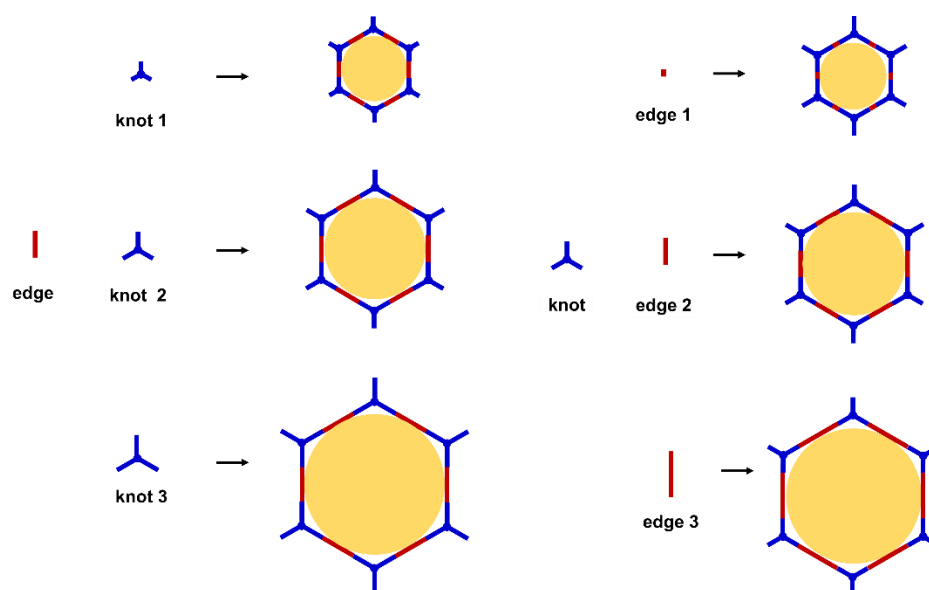


Figure 2. Modulating the pore size of the COFs.

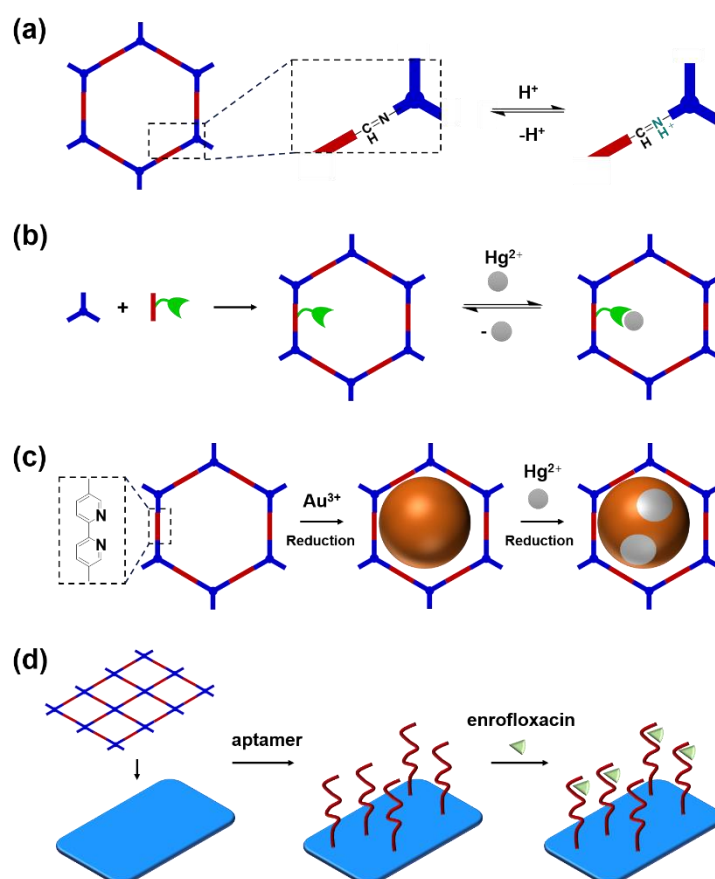


Figure 3. Introducing the binding site that can selectively capture the analyte. (a) capturing H^+ by imine linkage; (b) Intruding thioether binding site for capturing Hg^{2+} ; (c) Introducing AuNPs by in situ growth for mercury capture; (d) Externally immobilizing enrofloxacin-targeted aptamer onto the 2D sheet of the COF for capturing enrofloxacin.

2.2. Signals Produced by the Adsorption of the Analyte

Apart from the selective uptake and enrichment of the analyte, the other key problem in constructing a COF-based sensor is to make the uptake of the analyte produce a de-

tectable signal. By ingenious structural design, a large number of COFs of which the color, fluorescence, conductivity or capacitance can quantitatively change with the uptake of the analyte have been synthesized [18]. Besides that, in some reports the adsorption of the analyte can also produce some detectable signals which do not originate from COFs [29,50]. In this section, we will briefly discuss the generation, application, and advantages of the above signals in COF-based sensors. In addition, other analytical techniques such as QCM, Raman spectra, MS, et al. were also used occasionally. These techniques will be discussed with the particular examples demonstrated in the next section.

2.2.1. Fluorescence

Among the detectable signals caused by the uptake of the analyte, fluorescence change of COFs including fluorescence enhancement (“turn on”) and fluorescence quenching (“turn off”) is the most frequently used to respond to the concentration of analyte. Due to the rigid structure, the large π -conjugated fluorescent chromophores, such as phenyl, naphthalenyl, pyrenyl, perylenyl, triazine, and triphenyl-benzene are usually applied for building COFs [51,52]. Moreover, the conjugated linkages like imine and olefins can further enlarge the π -conjugated structure in the COFs. Therefore, it is not unusual to find a COF with fluorescent emission. However, it was found that the adsorption of some analytes may influence the fluorescent emission, including the change of the intensity and movement of the emission peak. The fluorescence change may be induced by various mechanisms, such as the charge and energy transfer between the COF and analyte, aggregation-induced emission, and exciplex formation, et al. The most common one among the above mechanisms is the charge transfer from an electron-rich COF to an electron-deficient analyte. It can lead to a significant fluorescent quenching which is relative to the concentration of the analyte. In the following demonstration, it can be found that many COF-based nitroaromatic explosive sensors, iodine sensors, and transition metal ions sensors are constructed by the charge transfer mechanism.

2.2.2. Chromism

Chromism is a signal that can be directly found by naked eyes. The advantage of the sensing approach based on chromism is easy-operate. It is very convenient to be further developed into rapid testing equipment like test paper, test kit, and wearable monitoring devices. Therefore, the COF-based sensors based on chromism are frequently reported. The color change of the COFs can be induced in different manners. Firstly, the non-covalent interaction between COFs and the analyte disturbs the electronic transition responsible for the coloration. For example, the adsorption of molecules with different polarities can influence the intramolecular charge transfer from the electron donor to the electron receptor on the COF skeleton, causing a red or blue shift of the UV-Vis absorbance [53]. Secondly, in some COF-based chromism sensors, the interaction with the analyte can isomerize some groups on the COF skeleton, resulting in the color change [54,55]. In addition, it should be noted that there is also a type of COF-based chromism sensor of which the color change is not caused by the COF itself. For example, in some sensors, COFs are used as a catalyst or a catalyst carrier, and the adsorption of the analyte can influence the catalytic capacity which can be detected by the formation of the colored product. Thus, the concentration of the analyte can be determined by the color change [29,50].

2.2.3. Capacitance and Conductivity

The adsorption of the analyte can lead to a change in the capacitance and conductivity of the COFs [56–58]. Hence the concentration of the analyte can be also determined by the change of such two electrical signals. In general, the quantitative measurement of electrical signals is much more convenient compared with photo signals. The measuring devices involved are much simpler. Therefore, COF-containing sensors based on the change of capacitance and conductivity are more likely to be realized on a chip-like device. Many presented works have demonstrated that a fingertip-size interdigital electrode (IDE) coated

with a specific COF can be applied for real-time detection of humidity, corrosive gases, or toxic gases since their adsorption results in the change of the capacitance or conductivity of the COFs. It can be expected that such a type of device can be further developed into portable, wearable, or even implantable sensors for real-time sensing.

2.2.4. Electrochemical or Photoelectrochemical Signals

Electrochemical or photoelectrochemical signals are generated by the redox reaction of the active substance. Plenty of analytical techniques based on electrochemistry or photoelectrochemistry have been built. The signal produced by electrochemical or photoelectrochemical reactions can be influenced by many factors such as the concentration of the active substances, the conductivity of the electrode/electrolyte interface, the existence of catalysts, and so on. In recent years, a number of examples of electrochemical or photoelectrochemical analysis with the participation of COFs were reported. The COFs coated on the electrode in these examples can play various roles including: (1) enriching the analyte that can be directly detected by the electrochemical or photoelectrochemical method; (2) concentrating the analytes to inhibit or facilitate the transportation of charges or substances; (3) a carrier for immobilizing the catalyst which adsorption can be affected by the analytes. All of the above allow a significant influence of the analyte on the electrochemical or photoelectrochemical signal. Compared with the above type of COF-based sensors the advantage of the electrochemical or photoelectrochemical signal is the high sensitivity. It is not rare to realize trace amounts of the analyte at or lower than ppb or ng/mL level with this type of COF-based sensor.

3. Application of COFs for Sensing Various Analytes

3.1. Gas Sensing

Generally, the key challenge of gas sensing is to capture the target molecule from the sample. Therefore, porous materials like zeolite, MOFs, and COFs show a great advantage in gas sensing. Driven by the increasing demand for healthcare and environmental protection, some COFs that can be used for detecting irritating, harmful, or toxic gases have been developed (Table 2).

3.1.1. Acidic and Alkaline Gases

Ammonia is widely applied in agriculture, the chemical industry, and refrigerated storage. Ammonia leakage can lead to discomfort and do harm to health. Although the pungent odor of ammonia can put us on high alert immediately, slow leakage of ammonia will decrease our sense of smell to find it. Therefore, it is necessary to detect trace amounts of ammonia. Early in 2010, O. M. Yaghi reported that the boronate linkage for synthesizing COFs can be used for ammonia uptake due to the Lewis acid–base interaction [59]. In 2016, D. Jiang and coworkers reported a highly emissive covalent organic framework (TPE–Ph–COF) based on dynamic boronate linkage [60] (Figure 4a). The boronate linkages can serve as a Lewis acid when it interacts with ammonia, which is a Lewis base. The interaction with ammonia significantly decreased the luminescence of TPE–Ph–COF. Hence, the dispersion of TPE–Ph–COF in organic solvent, such as toluene or cyclohexane, can be used for ammonia sensing. It can be found that the fluorescence of TPE–Ph–COF linearly decreased with the concentration of NH_3 and 1 ppm NH_3 could lead to a 30% reduction in fluorescence intensity. This result indicated that TPE–Ph–COF is a good candidate for detecting trace amounts of ammonia.

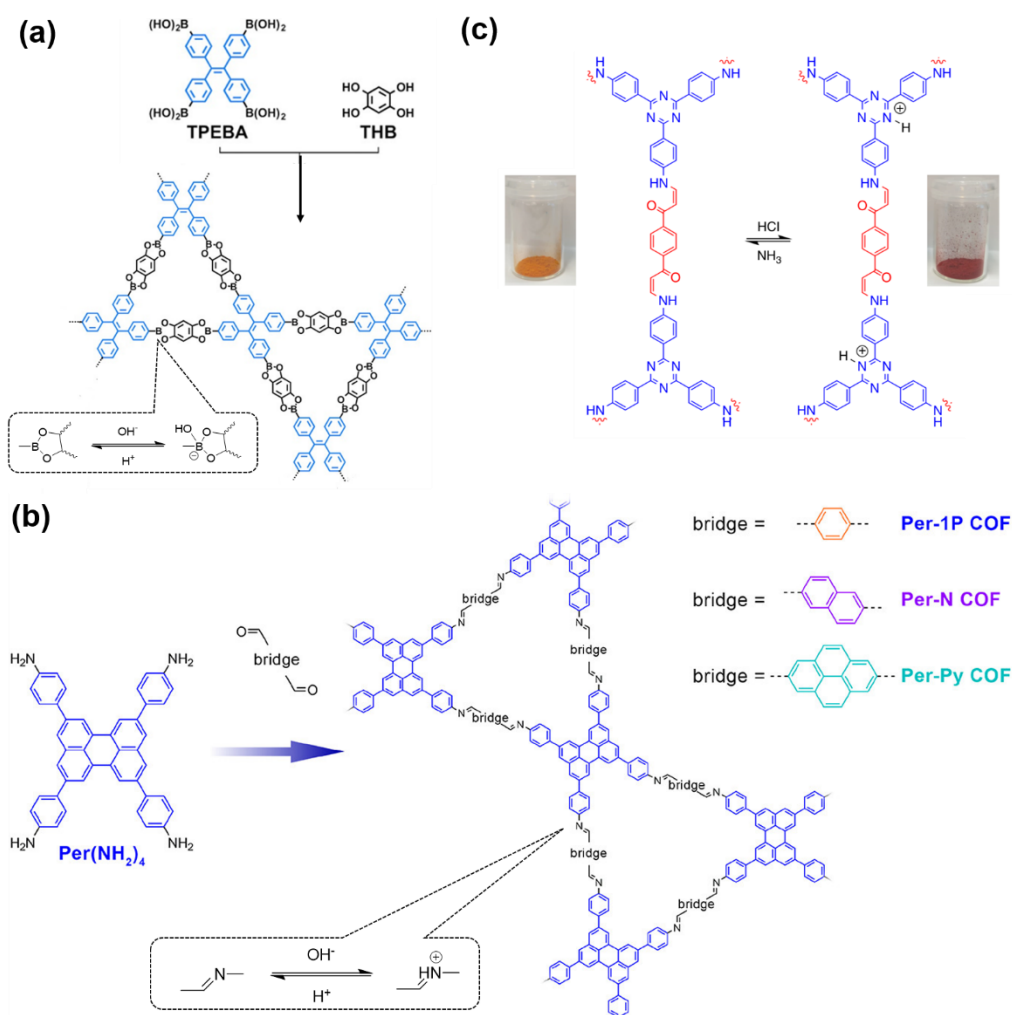


Figure 4. (a) COF for NH_3 sensing based on the protonation and deprotonation of boronate linkage [60]. Copyright 2016 American Chemical Society; (b) COF for HCl sensing is based on the protonation and deprotonation of imine linkage [47]. Copyright 2019 American Chemical Society; (c) COF for HCl, NH_3 sensing based on the protonation and deprotonation of imine linkage [57]. Copyright 2019 Nature Publishing Group.

It can be found that the acid–base interaction between NH_3 and the skeleton of the COFs played an essential role in NH_3 detection since NH_3 is a typical alkaline gas [60–65]. Correspondingly, it can be expected that acidic gas, such as HCl and TFA, can also be detected in a similar vein [47,48,57,62,66]. As with the boronate bond, the imine bond (Schiff base) is another frequently used dynamic linkage for COF synthesis. However, the imine linkage in COFs is usually a proton receptor that can easily react with acidic gases, allowing imine-based COFs to be sensitive to acids [47,66]. For example, F. Auras and co-workers developed a series of star-shaped COFs (Per-1P, Per-N, and Per-Py COFs) via the condensation of perylene tetraaniline with the phenylene-, naphthalene-, or pyrene-based dicarbaldehydes (Figure 3b) [47]. They found that the imine linkages of the star-shaped COFs can be reversibly protonated, resulting in a marked color change of the COFs. For example, the color of the Per-N-COFs thin film quickly changed from yellow to dark brown upon exposure to the vapor of trifluoroacetic acid (TFA). Its adsorption band around 385 nm decreased with the concentration of TFA vapor, simultaneously a new increasing absorption band around 450 nm could be observed. As a colorimetric acid vapor sensor, the detection limit of Per-N-COFs to trifluoroacetic acid can be as low as $35 \mu\text{g L}^{-1}$ and the response range was at least four orders of magnitude.

Table 2. COF-based gas sensing.

| Analyte | Year | COF Names | Specific Binding Site | Type of Detectable Signal | Detection Range | LOD | Reference |
|------------------|------|----------------------|-----------------------|---------------------------|------------------------------|-------------------------------|-----------|
| NH ₃ | 2016 | TPE–Ph–COF | Boronate | Fluorescence (turn off) | - | sub ppm level | [60] |
| | 2018 | HMP–TAPB–1HMP–TAPB–1 | Heptazine | conductivity | 1–200 ppm | 1 ppm | [61] |
| | 2018 | COP–COP–1 | Triazine | Fluorescence (turn on) | - | 5.8925×10^{-4} mL/mL | [62] |
| | 2019 | Ph–An–COF | Boronate | Fluorescence (turn off) | - | - | [63] |
| | 2019 | COF–DC–8 | - | Conductivity | 2–80 ppm | 56.8–70 ppb | [64] |
| | 2021 | TAPB–BPDA COF | Imine | Conductivity | 5–100 ppm | 10 ppb | [65] |
| TFA | 2019 | Per–N COF | Imine | Chromism | 0.035–110 mg L ⁻¹ | 35 µg L ⁻¹ | [47] |
| HCl | 2018 | COP–COP–1 | Triazine | Fluorescence (turn off) | - | 1.0967×10^{-4} mL/mL | [62] |
| | 2019 | PBHP–TAPT COF | Triazine | Chromism, conductivity | 20–3000 ppm | 20 ppm | [57] |
| | 2019 | COF–ETBA–DAB | Imine | Fluorescence | - | 4.7 ppm | [66] |
| | 2020 | BCTB–BCTA COF | Imine | Fluorescence (turn off) | 1–25 mM | 10 nM | [48] |
| H ₂ O | 2013 | TAPP–DHNDA–COF | Iminol | Chromism | 20–100% RH | - | [54] |
| | 2017 | COF–TXDBA | Boronate | Conductivity | 11–98% RH | - | [56] |
| | 2018 | Py–TT COF | - | Chromism | 0.64–0.98 p/p ₀ | - | [53] |
| | 2020 | TAPB–PDA–OH COF | Iminol | Chromism | - | - | [55] |
| | 2021 | DUT–175 | Imine | Chromism | 33–94% RH | - | [67] |
| Benzene | 2020 | BTA–TAPT-COF | Aromatic group | Capacitance | 500 ppb–100 ppm | 340 ppb | [58] |
| NO ₂ | 2019 | COF–DC–8 | - | Conductivity | 2–40 ppm | 1–16 ppb | [64] |
| | 2020 | CON–10 | - | Conductivity | - | 2.242 ppb | [68] |
| | 2020 | T–2DP | - | Conductivity | 0.15–5 ppm | 2.2 ppb | [69] |
| | 2021 | NiPc–CoTAA | - | Conductivity | 1–40 ppm | - | [70] |
| NO | 2019 | COF–DC–8 | - | Conductivity | 0.02–40 ppm | 1–5 ppb | [64] |
| H ₂ S | 2017 | PNT–1 | Triazine, pyridine | Fluorescence (turn off) | - | 53 ppb | [71] |
| | 2019 | COF–DC–8 | - | Conductivity | 2–80 ppm | 121 ppb | [64] |
| O ₃ | 2021 | P–COFTPb–DMTP–COF | imine | Chromism | - | 0.1 ppm | [72] |

Apart from the imine bond, triazine is another acid-sensitive group that has been frequently used in the fabrication of covalent organic porous materials. The long pair of three N atoms in triazine is a good H^+ acceptor. In 2018, N. Xu and coworkers prepared a high-performance fluorescent triazine-based covalent organic polymer (COP–COP–1) sensor for detecting both HCl and NH_3 gases [62]. It was found that when the COP–COP–1 was exposed to gaseous HCl, a redshift of the fluorescence happened and the intensity of the fluorescence decreased linearly with increasing HCl concentration. Conversely, NH_3 can lead to recovery of both color and fluorescence of the COP–COP–1 saturated by HCl, indicating that COP–COP–1 saturated by HCl can be applied as NH_3 detection. Later, R. Kulkarni and coworkers reported a triazine-based COF (PBHP–TAPT COF) with similar property [57] (Figure 3c). Gaseous HCl can protonate the triazine groups in PBHP–TAPT COF and quickly turn its color from yellow to red. A very low concentration of HCl (20–50 ppm) can result in a detectable color change. The reverse color switch can be realized by the deprotonation by NH_3 . Furthermore, R. Kulkarni and coworkers found that the protonation of the triazine groups enhanced the conductivity of PBHP–TAPT COF by 170-fold, indicating that apart from the colorimetric method the acidic gas detection by PBHP–TAPT COF can be conducted by also monitoring electrical conductivity.

Notably, the COF-based detection of NH_3 without acid–base interaction was also reported [65]. In 2021, F. Niu and coworkers synthesized a COF (TAPB–BPDA) via the condensation of 4,4'-biphenyldicarboxaldehyde with 1,3,5-tris(4-aminophenyl)benzene catalyzed by a proper amount of $Sc(OTf)_3$ and coated it onto an IDE. It can be measured that the resistance of TAPB–BPDA decreased when it was exposed to NH_3 . The limit of detection (LOD) of this resistance-based approach can be as low as 10 ppb. Meanwhile, owing to the hydrogen bond between the COF and analyte, the NH_3 sensing of TAPB–BPDA exhibited a good selectivity. Other gases, such as NO_2 , NO, SO_2 , H_2S , H_2 , CO, CO_2 , et al., cannot result in the resistance decrease. The work by F. Niu and coworkers provide an example of NH_3 sensing with noncovalent interaction.

3.1.2. Water Vapor (Humidity) Sensing

Humidity is one of the essential indexes of our working and living environment. The equipment for real-time humidity monitoring can be widely found in laboratories and factories. In recent years, developing wearable respiratory monitoring devices has drawn much attention in the fields of healthcare and sports, because they can be used to record the breathing rate and depth of patients and athletes. For fabricating a wearable respiratory monitor, a sensitive humidity responsive material is vital. Due to the designable pore structure, COFs are good candidates for selectively capturing and detecting water vapor in the air [53–56,67].

The mechanism firstly used for humidity detection is the keto-iminol tautomerism. Early in 2013, X. H. Liu and coworkers solvothermally prepared crystalline COF (TAPP–DHNDA–COF) nanofibers by the imine condensation between 2,4,6-tris(4-aminophenyl)pyridine (TAPP) and 2,6-Dihydroxynaphthalene-1,5-dicarbaldehyde (DHNDA) [54]. SEM images showed that the nanofibers can form when the time of solvothermal synthesis was longer than 24 h. By using aramid fabric as a nucleating agent, X. H. Liu and coworkers successfully prepared a TAPP–DHNDA–COF/aramid hybrid material, where TAPP–DHNDA–COF nanofiber was coated on the surface of the aramid fibers. The hybrid material exhibited a reversible colorimetric humidity-sensitive property because the addition of H_2O can disturb the equilibrium of keto-iminol tautomerism (Figure 5a). The color of the hybrid can switch from yellow to red gradually with the increasing relative humidity (R.H.) from 20% to 100%. Similarly, L. Ascherl et al. reported orienting a thin film formed by a tetrakis(4-aminophenyl)pyrene-based COF (Py–TT COF) (Figure 5b) [53]. The thin film exhibited a high humidity sensitivity. UV–Vis spectra revealed that a new absorption band between the 520–640 nm appeared after the exposure to enough $H_2O(g)$ and the original absorption across the 440–500 nm and 280–380 nm spectral regions simultaneously decreased. The highest sensitivity towards humidity appeared between H_2O relative

pressures of 0.64 and 0.79. Further investigation suggested that the mechanism of the color change is solvatochromism. Notably, the color change from a dry to humid atmosphere cost only 0.21s, and the converse procedure was even faster, when only 0.15 s was needed. It indicated that Py–TT COF thin film was potential material for real-time chromic humidity monitoring. Similarly, S. Jhulki and coworkers also reported a COF (TAPB–PDA–OH COF) containing 2,5-di(imine)-substituted 1,4-dihydroxybenzene (diiminol) moieties [55]. H₂O molecules can be adsorbed in the 1D channel of TAPB–PDA–OH COF via hydrogen bond. The adsorption of H₂O molecules resulted in the color of TAPB–PDA–OH COF changing from orange to dark red (Figure 5c). The response to the humid air cost only 9 s and the recovery procedure needed less than 1 s, indicating that TAPB–PDA–OH COF is also a good candidate for real-time humidity sensing.

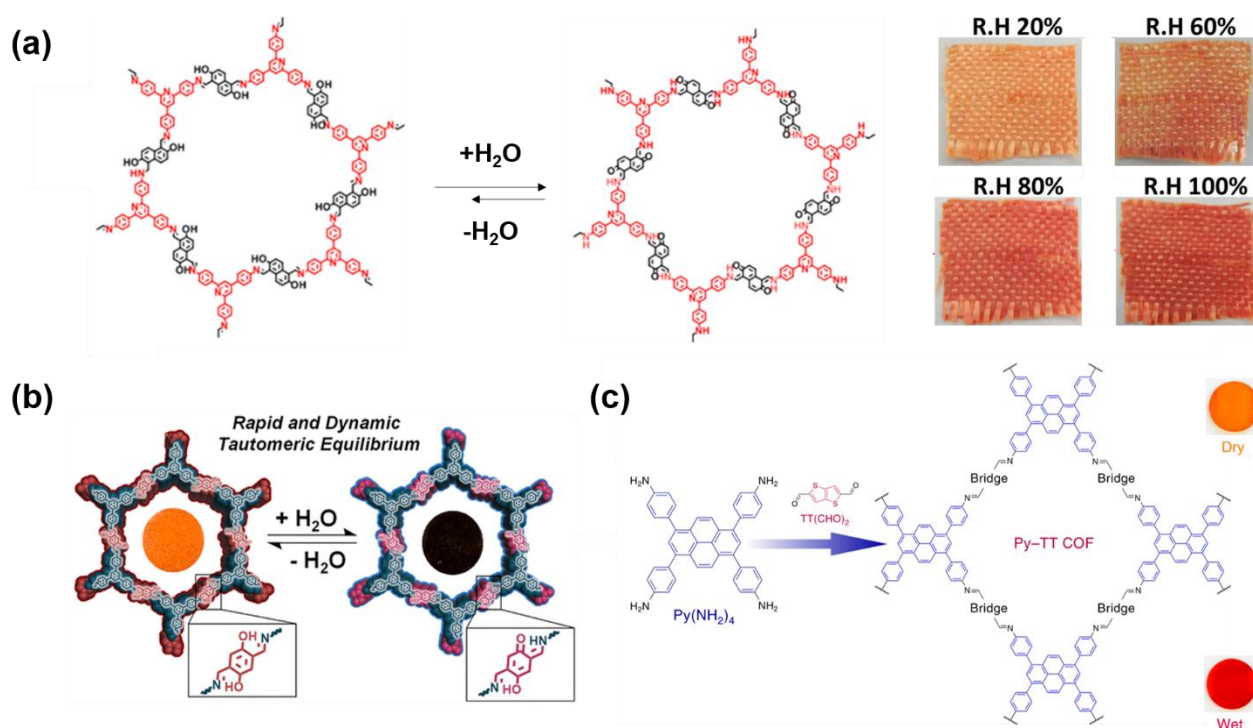


Figure 5. (a) TAPP–DHNDA–COF/aramid hybrid material for humidity detection [54]. Copyright 2013 American Chemical Society; (b) Py–TT COF thin film for humidity detection [53]. Copyright 2018 Nature Publishing Group; (c) Py–TT COF for humidity detection [55]. Copyright 2020 American Chemical Society.

In addition to color change, the adsorption of water vapor can also induce a decrease in impedance. H. Singh and coworkers synthesized truxene-based COFs with boron ester linkages (COF–TXDBA) [56]. The empty orbitals of the boron atom in the COF skeleton allowed the adsorption of H₂O via the Lewis acid–base interaction with the electron lone pair of the oxygen atom in the H₂O molecule. When R. H. was low, the amount of H₂O molecules was too low to form a continuous layer, hindering the charge transportation process among the water molecules by the Grotthuss chain reaction ($\text{H}_2\text{O} + \text{H}_3\text{O}^+ \rightarrow \text{H}_3\text{O}^+ + \text{H}_2\text{O}$). The conductivity of the COF–TXDBA was very low. However, if the amount of H₂O molecules allowed the formation of the continuous water layer and occurrence of the Grotthuss chain reaction, the impedance would sharply decrease. A linear relationship between R. H. and the logarithm of the impedance can be found in the range of R. H. 11 to 98%. Compared with the above-mentioned chromic method, the humidity sensing based on electrical impedance reported in this study was more quantitative and accurate. However, this approach also displayed a shortage. Its response time was measured as about 40 s, which is much longer than that of the chromic humidity sensor mentioned above.

3.1.3. Harmful Gases Sensing

With the development of the industry, the number of pollution incidences resulting from harmful gases has been increasing in recent decades. For example, the huge coal or oil consumption releases massive amounts of sulfur oxides and nitrogen oxides into the atmosphere, resulting in the high frequency of acid rain. In the indoor environment, the harmful gases released by some shoddy decoration materials such as benzene and formaldehyde are endangering human health seriously. The huge demand for alerting about harmful gases is promoting the development of the COFs for sensing levels of harmful gases.

As shown in Figure 6a, D. Zhao developed a COF-based chip-like device for benzene vapor sensing [58]. The device was prepared by in situ growing the film of a COF (BTA–TAPT–COF) which was synthesized by the imine condensation between benzene-1,3,5-tricarboxaldehyde (BTA) and 2,4,6-tris(4-aminophenyl)-1,3,5-triazine on an IDE. The exposure to benzene vapor significantly enhanced the capacitance of the device, which can be detected by an LCR bridge. The limit of benzene detection can reach 340 ppb. Notably, due to the interaction between electron-rich benzene and the electron-deficient triazine group, the COF-based benzene sensors showed good selectivity toward benzene over CO₂, CH₄, and C₃H₈ at room temperature. It suggested that the performance of the capacitive benzene sensor cannot be interfered by common indoor gases.

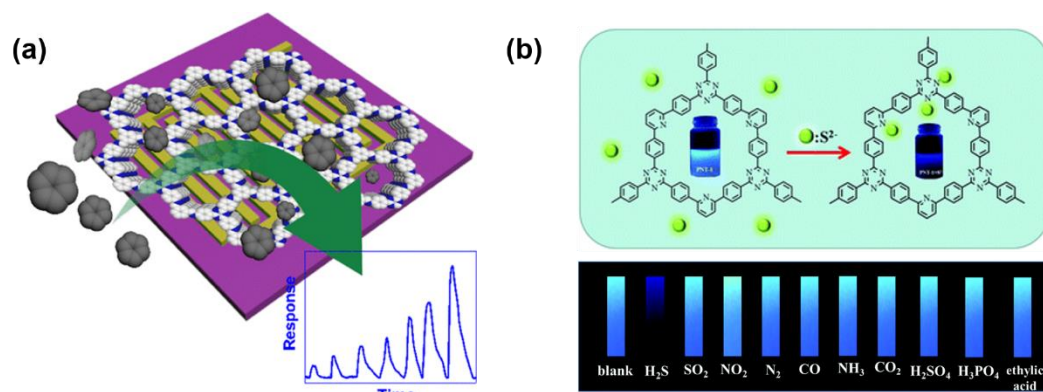


Figure 6. (a) COF-based IDE sensor for benzene vapor sensing [58]. Copyright 2020 American Chemical Society; (b) COF-based H₂S detection [71]. Copyright 2017 Royal Society of Chemistry.

Among various nitrogen oxides, the detection of NO₂ drew the most attention, because it is the most likely to appear in the atmosphere. For NO₂ sensing, the electrical method based on IDE was also applied [64,68,69]. K. A. Mirica and coworkers prepared a COF-coated IDE of which the resistance is sensitive to several harmful gases, including NH₃, H₂S, NO, and NO₂ [64]. The quantitative detection of these gases was realized. The LOD to these gases can reach the level of ppb. However, selective sensing of NO₂ had not yet been realized. Subsequently, D. Xia and coworkers fabricated a selective NO₂ sensor by drop-casting a triazine-based 2D organic polymer (T–2DP) on a gold IDE [69]. The T–2DP was prepared by the exfoliation of a covalent triazine framework synthesized through a triflic acid catalytic cyclotrimerization of 1,4-dicyanobenzene. The T–2DP sensor displayed a good performance in sensing trace amounts of NO₂. The linear range was < 1 ppm and the theoretical LOD is estimated to be 2.2 ppb. The sensor also showed a fast response to the analyte (response time: 35–47 s, recovery time: 56–140 s) and excellent selectivity. This work provided an example of selective high-performance NO₂ sensing.

In 2017, L. Guo and coworkers reported luminescent organic polymer nanotubes (PNT–1) for S^{2−} sensing [71]. The nanotubes were formed by a 2D structure synthesized by the condensation of 2,4,6-tris(4-bromo-phenyl)-1,3,5-triazine with 2,6-dibromopyridine. As shown in Figure 6b, the fluorescence of the PNT–1 suspended in CH₃OH can be quenched by adding Na₂S. The limit of the “turn off” fluorescent S^{2−} detection of PNT–1 was measured as 53 ppb. Other anions including halide ions, SO₄^{2−}, NO₃[−], HSO₃[−], PO₄^{3−},

CO_3^{2-} , et al. cannot result in the same phenomenon, indicating the good selectivity of the S^{2-} sensing. However, more importantly, Guo and coworkers subsequently further prepared a test paper for gaseous H_2S detection by dipping a piece of filter paper into the nanotube suspension for a few minutes (Figure 6b). It was found that the fluorescence of the newly prepared moist test paper can be immediately quenched upon exposure to the H_2S atmosphere. It indicated that fast detection of gaseous H_2S can be realized by PNT-1.

Very recently, a COF-based fast detection of ozone, which is an air pollutant brought by excessive emission of nitrogen oxides, was reported by Z. J. Zhang et al. [72]. The COF used for O_3 sensing is the frequently-reported TPB-DMTP-COF which was synthesized by 2,5-dimethoxyterephthalaldehyde and 1,3,5-tris-(4-aminophenyl) benzene. In the absence of moisture, ozone can nucleophilically attack imine groups to form nitro, aldehyde, and carboxylate moieties, while in the presence of moisture (R. H. = 40%) imine groups prefer to bind with water molecules to facilitate its protonation, leading to the visible color change from light yellow to red. Furthermore, the author found that TPB-DMTP-COF exhibited a better capacity of ozone removal than other porous materials such as activated carbon, amorphous polymer, monomer, and MOFs.

3.2. Inorganic Ions Sensing

3.2.1. Metal Ions Sensing

The concentrations of some metal ions, such as Fe^{2+} , Zn^{2+} , Mg^{2+} , et al., are important indicators of the health of human beings. For example, the analysis of $\text{Fe}^{2+}/\text{Fe}^{3+}$ has great significance in the diagnosis of anemia. Beyond that, heavy metal ions, such as Cu^{2+} , Hg^{2+} , Pb^{2+} , et al., are important industrial pollutants. Excessive heavy metal ions in water sources, food, or drink can cause serious poisoning and irreversible damage to human bodies. Therefore, the simple, rapid, accurate, and sensitive detection of all kinds of metal ions is widely expected in the fields of healthcare, environmental protection, and the food industry. Owing to the unique features of structural designability and selective absorbability, a variety of COFs have been designed for sensing a wide range of metal ions (Table 3).

Hg^{2+} is highly toxic and its existence in natural water or food must be particularly monitored. In 1956, the bioaccumulation of Hg^{2+} from industrial discharge caused the emergence of Minamata disease and finally resulted in a well-known social pollution nuisance. Therefore, many efforts have been devoted to the sensitive detection of Hg^{2+} in water. In general, for designing a COF that can effectively capture Hg^{2+} , special groups that can particularly bind with Hg^{2+} , such as thiol or thioether, were usually introduced [29,42,73,74]. The high affinity between S and Hg can significantly enhance the capacity of mercury uptake. In 2016, W. Wang et al. reported a fluorescent COF (COF-LZU8) with a hexagonal pore containing thioether group as a selective Hg^{2+} receptor [42]. The electron transformation from COF-LZU8 to Hg^{2+} can result in a markable fluorescence quenching, and the intensity of fluorescence linearly decreased with the concentration of Hg^{2+} (Figure 7a). The LOD was measured as 25.0 ppb. More importantly, the fluorescence quenching exhibited a significant selectivity, except for Hg^{2+} , fluorescence quenching caused by a wide range of metal ions is insignificant. Meanwhile, due to the excellent Hg^{2+} uptake capacity, COF-LZU8 can also be easily used for mercury (II) removal. Moreover, upon the simple treatment with concentrated Na_2S solution, COF-LZU8 can be easily recovered for the next Hg^{2+} detection and removal.

Table 3. COF-based ion sensing.

| Analyte | Year | COF Names | Specific Binding Site | Type of Detectable Signal | Detection Range | LOD | Reference |
|------------------|-----------|-------------------------------|-----------------------------|----------------------------------|-----------------------------|--------------------------------------|-----------|
| Hg ²⁺ | 2016 | COF-LZU8 | Thioether | Fluorescence, "turn off" | - | 25.0 ppb | [42] |
| | 2019 | TP-Bpy NSs | AuNPs | Chromism | - | 0.33 nM | [29] |
| | 2020 | TFPPy-CHYD | Carbohydrazide | Fluorescence, "turn off" | 0.05 μM-4 μM | 17 nM. | [73] |
| | 2021 | BATHz-Bt | Carbon-carbon double bonds | Fluorescence, "turn off" | 0-27.5 mM | 26 nM | [74] |
| Cu ²⁺ | 2016 | COF-JLU3 | Hydroxyl and azine | Fluorescence, "turn off" | 0-0.4 mM | 0.31 mM | [75] |
| | 2017 | CTF | Triazine | Chromism | 1.0 g/L-80.0 g/L | 0.05 g/L | [50] |
| | 2017 | LMOP-15LMOP-15 | Tertiary amino group | Fluorescence, "turn off" | | 5.1 × 10 ⁻⁸ M | [76] |
| | 2018 | sp2c-COFs | Cyano groups | Fluorescence, "turn off" | | 88 ppb | [77] |
| | 2019 | QG-scaffolded COF | N atoms and hydroxyl groups | Fluorescence, "turn off" | 0.0010~10.0 μM | 0.50 nM | [78] |
| Fe ³⁺ | 2017 | PI-COF 201 | Amino groups | Fluorescence, "turn off" | 5.0-400 μM | 0.13 μM | [79] |
| | | PI-COF 202 | | | 5.0-300 μM | 0.22 μM | |
| | 2019 | COF-TT | Amino groups | Fluorescence, "turn off" | 0-1.2 mM | 0.369 mM | [80] |
| | | TaDAP TaDA | | | Imine | 0.02-0.2 mM | 18 μM |
| | 2019 | Bth-Dha, Bth-Dma | O,N,O'-chelating sites | Fluorescence, "turn off" | - | 0.17 μM | [82] |
| | 2021 | TTPE-COF | | | Fluorescence "turn off" | 10 ⁻⁸ -10 ⁻² M | 3.07 μM |
| | 2021 | Tfpa-Mth COF | Hydrazide and phenol ether | Fluorescence, "turn off" and QCM | - | 64 nM | [84] |
| 2021 | PMDA-TAPB | Carbonyl group | Fluorescence, "turn off" | | - | - | [85] |
| Pb ²⁺ | 2018 | TAPB-DMTP-COF | Amino groups | Electrochemical signals | 0.0050-2.0 μM | 0.0019 μmol/L | [86] |
| | 2019 | Sulfhydryl modified | Sulfhydryl | Electrochemical signals | 0.05-20 ng·mL ⁻¹ | 0.015 ng·mL ⁻¹ | [87] |
| | | TAPB-DMTTAPB-DMTTAPB-DMTP-COF | | | | | |
| | 2021 | TAPP-COF | | Photoelectrochemical signal | 0.05-1000 nM | 0.012 nM | [88] |
| 2021 | PMDA-TAPB | Amino groups | Electrochemical signals | 5-9000 nM | 1.22 nM | [85] | |
| Au ⁺ | 2018 | TTB-COF | Thioether | Fluorescence, "turn on" | 1.0-10.0 mM | 1.39 mM | [89] |

Table 3. Cont.

| Analyte | Year | COF Names | Specific Binding Site | Type of Detectable Signal | Detection Range | LOD | Reference |
|-------------------------------|------|--------------------|----------------------------|---------------------------|--------------------------------------|-----------|-----------|
| UO ₂ ²⁺ | 2020 | TFPT–BTAN–AO | Carbon-carbon double bonds | Fluorescence, “turn off” | - | 6.7 nM | [90] |
| | 2021 | Tph–BDP | Imines of the CT complex | Chromism | 0.18–75 μM | 0.05 μM | [91] |
| Ni ²⁺ | 2021 | BPD–COFs | N atoms | Fluorescence, “turn off” | 0.420–1.26 × 10 ³ pM | 68.0 pM | [92] |
| Cr ³⁺ | 2021 | CoPc–PT–COF@Cu–MOF | Bipyridine | Electrochemical signals | 10 ⁻¹ –10 ⁵ pM | 0.0229 pM | [93] |
| Pd ²⁺ | 2021 | XB–COFs | Carbon-carbon double bonds | Fluorescence, “turn off” | - | 0.29 μM | [94] |
| | 2021 | PY–SE–COF | Selenodiazole | Fluorescence, “turn off” | 20–450 mM | 0.45 mM | [95] |

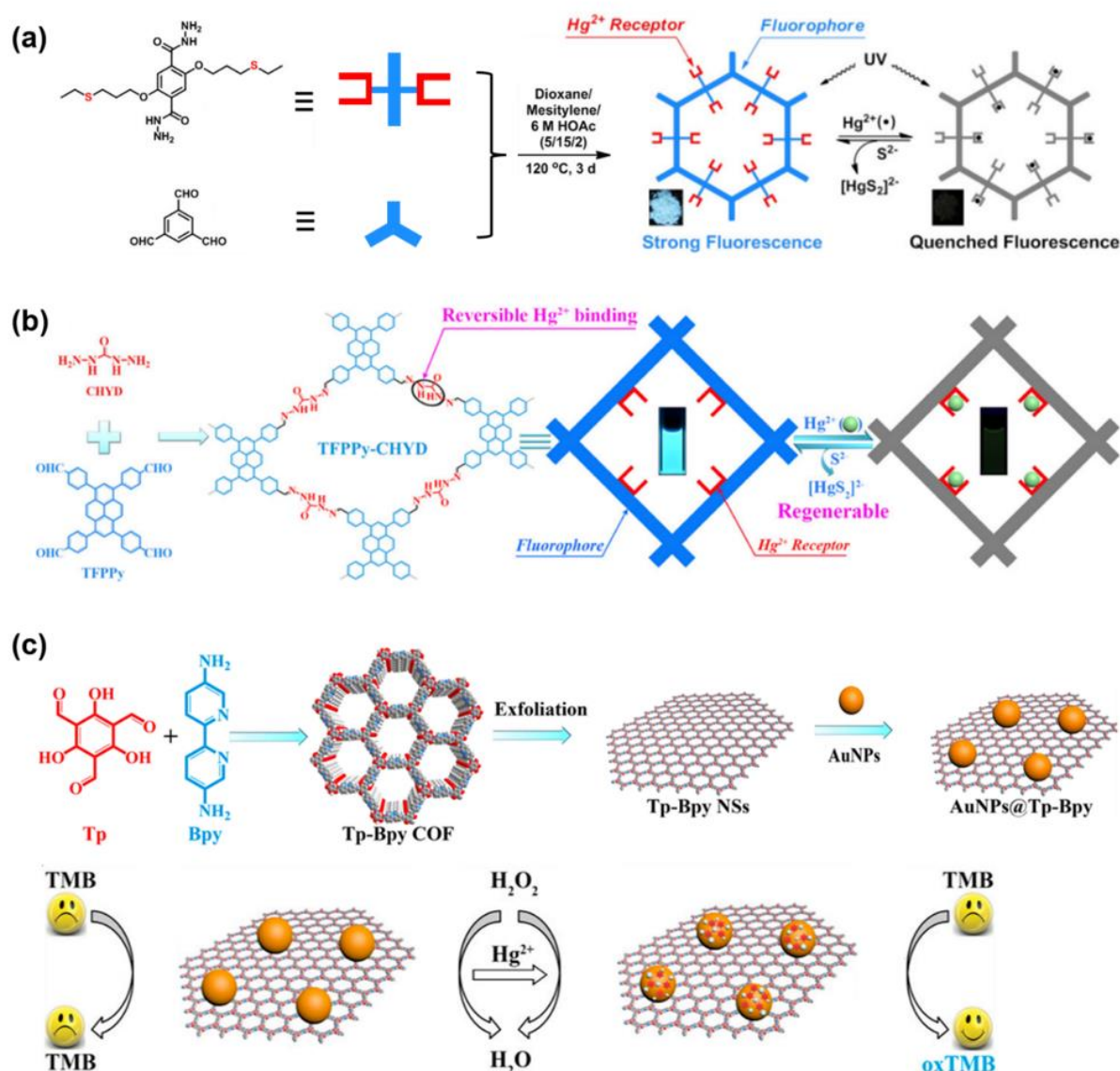


Figure 7. (a) COF-LZU8 for Hg²⁺ detection via fluorescence quenching [42]. Copyright 2016 American Chemical Society; (b) TFPPy-CHYD for Hg²⁺ detection via fluorescence quenching [73]. Copyright 2020 American Chemical Society; (c) Tp-Bpy NSs for Hg²⁺ detection via catalytic oxidation of TMB [29]. Copyright 2019 American Chemical Society.

In addition to the S(II) containing groups, it was reported that the carbohydrazide group can be also applied for capturing Hg²⁺ in the aqueous solution. J.-D. Qiu et al. designed a pyrene-based luminescent COF (TFPPy-CHYD) with a flexible carbohydrazide (CHYD) linkage [73] (Figure 6b). The CHYD group can effectively bond Hg²⁺ in the tetragonal pore of TFPPy-CHYD by coordination interaction. The maximum adsorption capacity for Hg²⁺ can be as high as 758 mg g⁻¹. The binding between Hg²⁺ and CHYD also exhibited good reversibility. The Hg²⁺ captured by TFPPy-CHYD can be effectively removed by 10 equiv. of Na₂S solution. In the meantime, the binding of Hg²⁺ led to a quick, efficient quenching of the fluorescence which cannot be found in presence of other metal ions. The intensity of the fluorescence decreased linearly with [Hg²⁺] when 0.05 μM < [Hg²⁺] < 4 μM. The LOD was measured as 17 nM.

Due to the high toxicity, the threshold level of mercury in drinking water is as low as 10 nM. Therefore, it is still necessary to develop Hg²⁺ sensors with lower LOD. As well as capturing Hg²⁺ into the pore of COFs, other strategies to detect trace amounts of mercury

have been also attempted. For example, J.-D. Qiu and coworkers reported a COF-based nanocomposite for Hg^{2+} sensing for which the LOD can be lower than 1 nM [29]. As shown in Figure 6c, they synthesized bipyridine-containing COF nanosheets, Tp–Bpy NSs, with a regular hexagonal pore structure. Due to the nitrogen-containing bipyridine groups, a large number of AuNPs can be doped onto the Tp–BpyTp–Bpy NSs by in situ growth method to form a AuNPs@Tp–Bpy nanocomposite. In citric acid-phosphate buffer solution, AuNPs@Tp–Bpy can adsorb trace amounts of Hg^{2+} from the sample solution to form a gold amalgam layer on the surface of the AuNPs. The amalgam layer allows H_2O_2 to be decomposed efficiently to form highly reactive hydroxyl radicals which can rapidly oxidize colorless 3,3',5,5'-tetramethylbenzidine (TMB) to its bright blue oxidation state (oxTMB). Hence, the absorbance at 652 nm caused by oxTMB can be used to quantitatively determine the concentration of Hg^{2+} in the sample solution. Notably, this approach for Hg^{2+} sensing exhibited an ultrahigh sensitivity. The color changes caused by even 1 nM Hg^{2+} were easily detected.

Apart from Hg^{2+} , the detection of Cu^{2+} , Fe^{3+} , and Pb^{2+} has also drawn much attention recently. Although the toxicity of Cu^{2+} is far less than Hg^{2+} , the widespread existence of Cu^{2+} may still risk the health of citizens. Therefore, COFs that can sensitively and selectively detect Cu^{2+} have been developed. The strategy to develop COFs for Cu^{2+} detection had much in common with COF-based Hg^{2+} sensing. In recent years, several luminescent COFs, of which fluorescence can be quantitatively quenched by the addition of Cu^{2+} , were presented. In 2016, X. Liu and co-workers synthesized a hydrogen bond-assisted azine-linked COF (COF–JLU3) with robust chemical stability and thermal stability [75]. It displayed a high luminescence efficiency due to the bulky *tert*-butyl groups on the skeleton, which can adjust the π – π interaction between the layers. The numerous N atoms and hydroxyl groups in the pore of COF–JLU3 acted as receptors to benefit the uptake of metal cations. It was found that transition-metal ions with different electron configurations such as Fe^{3+} , Co^{2+} , especially Cu^{2+} , can be captured resulting in significant quenching the fluorescence of COF–JLU3. The decrease of fluorescence emission intensity was almost proportional to $[\text{Cu}^{2+}]$ in the range from 0 to 0.4 mM, suggesting that COF–JLU3 is a suitable candidate for Cu^{2+} detection. The LOD of Cu^{2+} sensing was measured as 0.31 mM. In 2018, D. Jiang and coworkers designed and successfully synthesized a series of stable light-emitting two-dimensional sp^2 carbon-conjugated COFs (sp^2c -COFs) [77]. They exhibited excellent luminescence activity and high stability simultaneously. Interestingly, the –CN side groups in sp^2c -COFs were able to interact with Cu^{2+} resulting in the quenching of the luminescence. Only 88 ppb (about 1.4 μM) Cu^{2+} can result in an observable quenching. It indicated that sp^2c -COFs can serve as a highly selective and effective sensor for detecting Cu^{2+} ions. Later, H. Wang et al. reported a fluorescent QG–scaffolded COF synthesized by the one-step covalent reactions of melamine-aldehyde and phenol-aldehyde poly-condensations using paraformaldehyde, initially with Q-Graphene (QG) scaffolds [78]. The N atoms and hydroxyl groups on the COF skeleton can effectively chelate Cu^{2+} . Different from other metal ions, Cu^{2+} can significantly quench the fluorescence of QG–scaffolded COF, indicating that the QG–scaffolded COF is a good candidate for Cu^{2+} sensing. The linear range of the Cu^{2+} sensing was measured as 0.0010–10.0 μM and the LOD can reach 0.50 nM. Moreover, as with the Hg^{2+} detection, this strategy relies on the enzyme-mimicking property of nanomaterials can be also applied in Cu^{2+} detection. In 2017, Y. Xiong et al. developed a covalent triazine framework (CTF) that can exhibit peroxidase-like catalytic activity once it is coordinated with Cu^{2+} [50]. The copper ions acted as the active sites in the complex formed by CTF and Cu^{2+} (CTF/ Cu^{2+}). It can be found that the catalytic activity of CTF/ Cu^{2+} can be tuned by the concentration of Cu^{2+} . Upon the addition of H_2SO_4 , H_2O_2 , and TMB, the concentration of Cu^{2+} can be easily determined by UV-Vis absorbance. This colorimetric method showed good selectivity. Its linear range was measured as 1.0 $\mu\text{g}/\text{L}$ to 80.0 $\mu\text{g}/\text{L}$, and the LOD was determined as 0.05 $\mu\text{g}/\text{L}$.

Iron is one of the essential trace elements of the human body. It plays an important role in oxygen uptake and transfers into red blood cells. Iron is also an important part of some

enzymes, for example, catalase. Hence the detection of Fe^{3+} has important significance in the food industry and health examination. In recent years, a number of COFs that can be used for Fe^{3+} detection were reported [79–85]. Most of them were based on Ion-induced fluorescence quenching. In 2017, W. Yang and coworkers reported two polyimide-based porous COFs (PI–COF 201 and PI–COF 202) [79]. Owing to the p*-n transition caused by the high electro-delocalization and the inherently rigid structure, the two COFs can emit strong fluorescence. However, the adsorption of Fe^{3+} remarkably quenches their fluorescence due to the energy transfer from the emission level of the COFs to the unoccupied d-orbital of Fe^{3+} . A linear relationship between the fluorescence intensity and $[\text{Fe}^{3+}]$ was found in the range of 5.0–40 μM . The LODs were determined as 0.13 μM (PI–COF 201) and 0.22 μM (PI–COF 202), respectively. Later, several luminescent COFs of which fluorescence can be quenched by Fe^{3+} were reported [80–85]. The LOD of the COF-based Fe^{3+} sensing has been decreased to 64 nM. Notably, some COFs for Fe^{3+} sensing can be also used to detect other ions, such as Pb^{2+} [85], CrO_4^{2-} , $\text{Cr}_2\text{O}_7^{2-}$, and MnO_4^- [80]. Meanwhile, besides fluorescence quenching, COF-based Fe^{3+} sensing in another manner has been also reported. In 2021, W.-G. Zhang and coworkers prepared a robust hydrazone-linked COF (Tfpa–Mth COF), of which its fluorescence can be quenched by Fe^{3+} [84]. In the meantime, W.-G. Zhang and coworkers prepared a uniform Tfpa–Mth COF thin film on an amino-modified quartz crystal microbalance (QCM) chip by in situ growth method. The Tfpa–Mth COF thin film can capture Fe^{3+} , resulting in a frequency shift in QCM measurement. Compared with the fluorescence quenching, the Tfpa–Mth COF-coated QCM chip displayed a significant advantage in real-time Fe^{3+} monitoring.

Pb^{2+} is another metal ion with which COF-based sensing has been widely concerned. Similar to mercury, lead can be also accumulated in plants and animals and further threaten human beings through the food chain, resulting in irreversible damage to the liver, nervous or circulatory system. Even nowadays, lead is still widely used in batteries, gasoline additives, and paint pigments. Therefore, fast and sensitive lead sensing is still needed. Unlike Hg^{2+} sensing, the reported COF-based Pb^{2+} sensors were more likely to depend on electrochemical signals [85–88]. In 2018, Y. Wang and J. Wang [86] and co-workers mixed TAPB–DMTTAPB–DMTP–COF [85] with graphite powder to prepare a TAPB–DMTTAPB–DMTP–COF-based carbon paste electrode (TAPB–DMTTAPB–DMTP–COF/CPE) for sensitive and selective Pb^{2+} sensing. The huge surface area and a large number of amino groups of TAPB–DMTTAPB–DMTP–COF greatly benefited the capture of Pb^{2+} from the sample solution. By using TAPB–DMTTAPB–DMTP–COF/CPE, the concentration of Pb^{2+} can be determined by differential pulse stripping voltammetry. The change of current intensity showed excellent linearity to the concentration of lead in the range of 0.0050 to 2.0 μM and the LOD of this method was measured as 1.9 nM. Similarly, X. Wang and coworkers prepared an Au electrode coated with sulfhydryl-modified TAPB–DMTTAPB–DMTP–COF for Pb^{2+} detection [87]. The $[\text{Pb}^{2+}]$ was determined by square wave anodic stripping voltammetry with the electrode. Benefiting from the affinity between S(II) and Pb, the LOD of the Pb^{2+} detection can be as low as 0.015 ng/mL (0.072 nM). Recently, Y. Zhang et al. further enhanced the sensitivity of COF-based Pb^{2+} detection by introducing the photoelectrochemical (PEC) sensing technique [88]. They firstly prepared a photocathode by fabricating a porphyrin-based COF (TAPP–COF) on a PET-ITO electrode. The photocathode presented an outstanding photovoltaic property owing to the unique charge channels of COFs and the good photoelectric properties of porphyrin. Then the CdSe quantum dots coated with a SiO_2 shell (CdSe@SiO₂QDs), which herein acted as a quenching agent, were immobilized onto the TAPP–COF thin film through a hybridization chain reaction, significantly decreasing the photocurrent. However, the presence of Pb^{2+} can detach the CdSe@SiO₂QDs from the TAPP–COF thin film, leading to the quantitative recovery of the photocurrent. Hence, accurate sensing of Pb^{2+} can be achieved in a wide detection range of $[\text{Pb}^{2+}]$ (0.05–1000 nM) with an extremely low LOD of 0.012 nM.

In recent years, the interest in developing COF-based metal ion sensing has been gradually extended. In addition to the above-mentioned metal ions, the COFs for sensing other ions such as Au^+ , UO_2^{2+} , Ni^{2+} , Cr^{3+} , Pd^{2+} , et al. have been developed one after another. In 2018, Y. Yu designed and synthesized a thioether-functionalized fluorescent COF (TTB-COF) for selective sensing Au ions [89]. Observable fluorescence quenching of TTB-COF can be induced by adding Au ions. The fluorescence intensity and the concentrations of Au ions showed a linear relationship in the range of 1.0–10.0 mM and the LOD is calculated to be 0.87mM. In addition, TTB-COF exhibited a large capture capacity to Au ions (560 mg g^{-1}); thus, it is also a promising material for the recovery of ultra-low concentration Au ions in the aqueous solution. Uranium is one of the essential raw materials in the nuclear industry. However, its content in the earth's crust is quite low, therefore, porous materials for uranium extraction from seawater and detection of uranium have been recently focused on [90,96–99]. J.-D. Qiu and coworkers prepared a fluorescent COF (TFPT-BTAN-AO) containing a large amount of selective uranium-binding groups as shown in Figure 8a [90,91]. The TFPT-BTAN-AO can selectively capture UO_2^{2+} ions. The uptake capacity was measured as 427 mg g^{-1} , suggesting that it is possible to be applied for the purposes of uranium extraction. The fluorescence emission of TFPT-BTAN-AO linearly decreased upon the gradual addition of UO_2^{2+} . The LOD was determined as 6.7 nM. Similarly, Q. L. Deng and coworkers reported that a COF containing the bipyridine group in its skeleton of fluorescence can be selectively quenched by Ni^{2+} when pH = 10 [92]. As a platform for Ni^{2+} detection, an extremely low LOD of (68 pM) can be achieved. Meanwhile, the COFs have been also used for chromium sensing. As mentioned above, the COF for Fe^{3+} sensing reported by Z. Shi et al. [80] can also be applied for the detection of Cr(VI), which is a highly toxic carcinogen. Meanwhile, M. Du and coworkers prepared a COF-containing nanocomposite as a platform for the high-efficiency determination of Cr(III) [93]. As shown in Figure 8b, the nanocomposite (DNA/CoPc-PT-COF@Cu-MOF) was prepared by firstly growing two-dimensional phthalocyanine-based COF on Cu-MOF and then immobilizing DNA strands that can recognize Cr^{3+} . The DNA/CoPc-PT-COF@Cu-MOF was coated onto a glass carbon electrode (GCE), yielding a Cr^{3+} sensor. It was found that the binding with the Cr^{3+} enhanced the charge transfer resistance, R_{ct} , of the DNA strands, which can be detected by electrochemical impedance spectroscopy (EIS). In the meantime, DNA/CoPc-PT-COF@Cu-MOF also displayed a photoelectrochemical property. Cr^{3+} can result in a decrease in the photocurrent. Hence the Cr^{3+} can be detected by monitoring both R_{ct} and photocurrent. The calculated LOD of the Cr^{3+} biosensor was as low as 14.5 fM. Very recently, two fluorescent COFs that can selectively detect Pd^{2+} were reported by J.-Y. Yue et al. and Y. Lu. et al., respectively [94,95]. Their fluorescence can be selectively quenched by Pd^{2+} . Interestingly, the Pd^{2+} -sensitive COF by Y. Lu. et al. was prepared in situ on a piece of paper, yielding a COF-based test paper for Pd^{2+} detection. Considering the wide application of palladium in the industry, it can be expected that the Pd^{2+} test paper will show good practicability in the fast detection of the catalyst residual.

3.2.2. pH Sensing (H^+ Sensing)

Similar to the detection of the acidic/alkaline gases, introducing an acid/alkaline responsive group is the key to creating a COF for pH sensing (H^+ sensing in water). [100–104] Early in 2016, Y. Mu and X. M. Liu et al. reported a COF (COF-JLU4) with protonatable β -ketoenamine in its skeleton [104]. The fluorescence spectra of COF-JLU4 can gradually change with the pH value in aqueous solution, indicating that pH-responsive luminescent COFs can be a candidate for pH sensing. Subsequently, several COFs of which fluorescence is responsive to pH value were developed (Table 4) [101,103,104]. Notably, C. L. Zhang et al. synthesized an imine-linked fluorescent COF containing triazine groups (COF₂) [100]. The protonation of both imine linkage and triazine affected the intensity of fluorescence. Interestingly, the plot of fluorescence titration vs. pH showed a significant jump when pH = 6.5. It is suggested that COF₂ can be used in the detection of cancer as a fluorescent probe. Thus, C. L. Zhang et al. modified the 2D nanosheet of COF₂ with poly-D-lysine to

improve its dispersity in aqueous solution, biocompatibility, and endocytosis efficiency. The experiment result exhibited that COF₂ modified by poly-D-lysine can be successfully used in the in vitro cancer cell imaging and in vivo pH imaging in zebrafish.

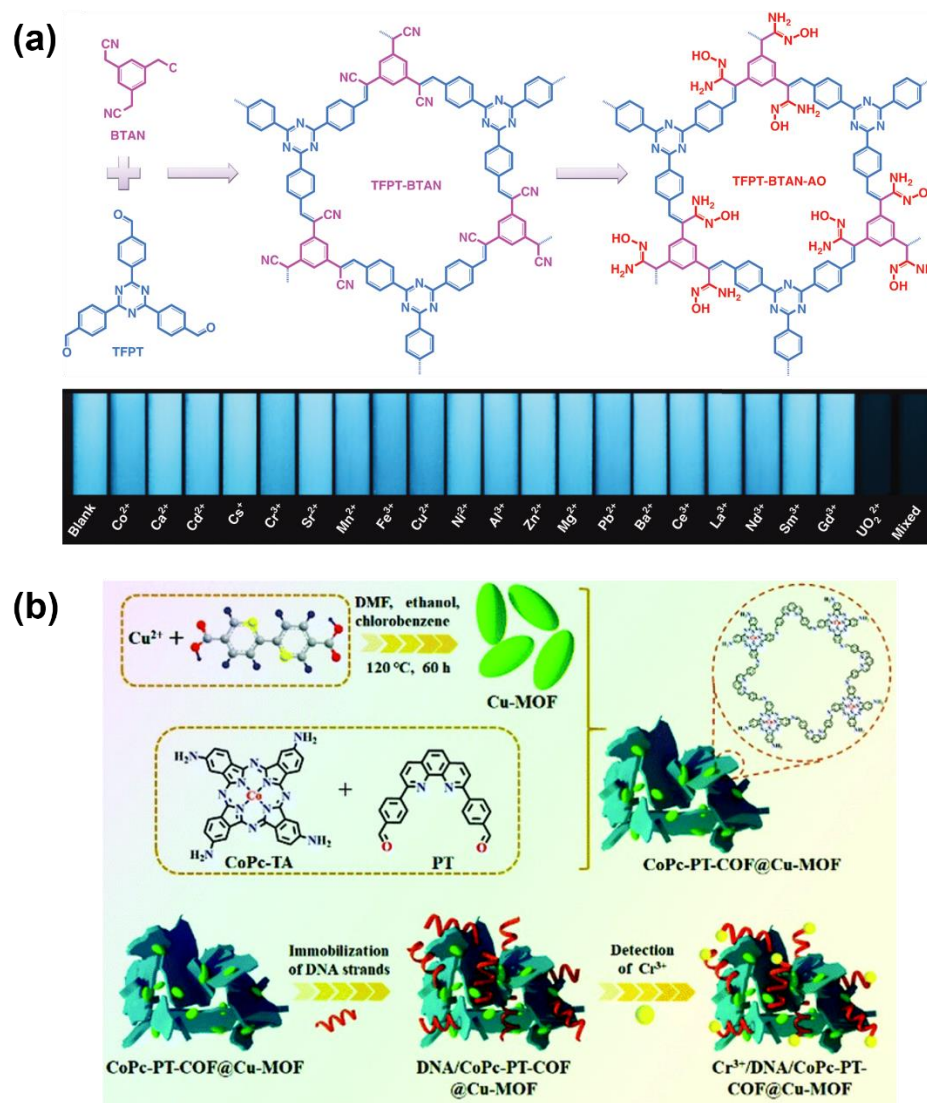


Figure 8. (a) TFPT–BTAN–AO for UO₂²⁺ detection via fluorescence quenching [90]. Copyright 2020 Nature Publishing Group; (b) DNA/CoPc–PT–COF@Cu–MOF nanocomposite for Cr³⁺ detection [93]. Copyright 2021 Royal Society of Chemistry.

In addition to fluorescent quenching, COF-based pH sensing can be conducted in other ways. For example, L. Wang and coworkers synthesized an imine-linked COF (COF_{DHTA-TTA}) with multiple redox-active states [102]. Owing to the redox activity, the COF_{DHTA-TTA} showed a good performance in catalyzing the decomposition of H₂O₂. Therefore, it can be expected that a COF_{DHTA-TTA} coated glassy carbon electrode (GCE) can be applied in the electrochemical analysis of H₂O₂. Additionally, the electron transport process of COF_{DHTA-TTA}/GCE was accompanied by H⁺ transfer. Thus, pH could be also determined by using COF_{DHTA-TTA}/GCE based on the peak potential as signal outputs. The experiment result showed that the peak potential exhibited a good linear relationship with the pH value of the solution in the experiment. In addition, the authors loaded glucose oxidase into the pores of COF_{DHTA-TTA}. It made the COF_{DHTA-TTA} coated GCE give a good performance for glucose detection.

Table 4. COF-based pH sensing.

| Analyte | Year | COF/COF Hybrid Names | Specific Binding Site | Type of Detectable Signal | Detection Range | Reference |
|----------------|------|-------------------------|-----------------------|---------------------------|-----------------|-----------|
| H ⁺ | 2016 | COF–JLU4 | Amine | Fluorescence “turn off” | pH 0.9–13.0 | [100] |
| | 2018 | COF–HQ | Quinoline | Fluorescence “turn off” | pH 1.0–5.0 | [101] |
| | 2019 | COF _{DHTA-TTA} | - | Electrochemical signals | pH 3.0–11.0 | [102] |
| | 2021 | COF ₂ | Imine or triazine | Fluorescence “turn on” | pH 5.0–8.0 | [103] |
| | 2021 | COF–TP | Amine | Fluorescence “turn off” | pH 0–6.0 | [104] |

3.2.3. Inorganic Anions Sensing

The inorganic anions in aqueous solution mainly include various acid radical ions. However, the COF for sensing inorganic anions was not frequently investigated as cations. Only a few reports can be found (Table 5). As mentioned above, the Fe³⁺ sensitive COF reported by Z. Shi et al. [80] can also be used for detecting CrO₄²⁻, Cr₂O₇²⁻, and MnO₄⁻ via fluorescence quenching. The detection of Cr(VI) is of practical value because it is a water pollutant with significant carcinogenicity. So far, the inorganic ion that attracted the most attention is F⁻ [103–105], because excessive F⁻ in drinking water can damage human teeth and bones.

Table 5. COF-based anion sensing.

| Analyte | Year | COF Names | Specific Binding Site | Type of Detectable Signal | Detection Range | LOD | Reference |
|--|------|-----------------|-----------------------|---------------------------|-----------------|----------|-----------|
| CrO ₄ ²⁻ (Cr ₂ O ₇ ²⁻) | 2019 | COF–TT | | Fluorescence, “turn off” | | 0.343 mM | [80] |
| MnO ₄ ⁻ | 2019 | COF–TT | | Fluorescence, “turn off” | | 0.320 mM | [80] |
| F ⁻ | 2015 | BCMP–3 | Boron sites | Fluorescence, “turn off” | | | [105] |
| | 2018 | TFPPy–DETHz–COF | Amine | Fluorescence, “turn off” | - | 50.5 ppb | [106] |
| | 2018 | 2D–Fe–CTF | Triazine | Chromism | 10–100 μM | 0.56 μM | [107] |
| S ²⁻ | 2018 | TpASH | Azide | Fluorescence, “turn on” | 1 μM–5 mM | 0.12 μM | [108] |

Early in 2015, X. M. Liu et al. reported on a boron-containing COF (BCMP–3) [105]. Unlike other anions, the Lewis acid–base interaction between the B atom and F⁻ can result in the change of fluorescence of BCMP–3 (Figure 9a). A remarkable blueshift and intensity decrease can be found upon the addition of F⁻. The BCMP–3 can be also used for F⁻ removal. The adsorption capacity was 24 mg/g. Subsequently, D. L. Jiang and his coworkers synthesized a luminescent COF (TFPPy–DETHz–COF) that can be used for F⁻ sensing [106]. They found that F⁻ can react with the N–H unit in the hydrazone linkage of TFPPy–DETHz–COF based on an acid–base reaction mechanism, while other halogen anions like Cl⁻, Br⁻, I⁻ were inert (Figure 8b). The reaction with F⁻ deprotonated the N–H bond to form an anionic nitrogen species which can eliminate the nitrogen-related fluorescence quenching pathway, leading to a remarkable enhancement of the fluorescence intensity. Therefore, TFPPy–DETHz–COF was a rare fluorescence switch-on sensor because its intensity increases as [F⁻] is increased. The detection limit of F⁻ detection was down to 50.5 ppb. Additionally, the F⁻ sensing based on the analogues of COFs, covalent triazine frameworks (CTF), was also reported. The F⁻ sensing can be conducted by the CTF in a pathway without fluorescence. In the same year, Y. H. Xiong demonstrated an iron-modified two-dimensional CTF (2D–Fe–CTF) which exhibited remarkable peroxidase-like activity. F⁻ can coordinate with the iron ion in the CTF and significantly decreased the enzyme-mimicking activity [107]. Therefore, the concentration of F⁻ can be detected by monitoring the rate of H₂O₂ decomposition. The LOD of this approach can be as low as 5 nM, and other anions such as Cl⁻, Br⁻, SO₄²⁻, NO₃⁻, HCO₃⁻, HCOO⁻, CO₃²⁻, PO₄³⁻, and CH₃COO⁻ did not show significant interference.

In addition to F^- , the COFs for sensing S^{2-} in solution have also been focused on [71,108], because H_2S can act as a signal transmission molecule in the human body, the same as NO and CO [109,110], and participates in some important pathophysiological processes such as neuromodulation and vasodilation. As demonstrated above, the organic polymer nanotubes PNT-1 can be used for detecting Na_2S in CH_3OH solution. Its fluorescent emission decreased with the addition of Na_2S . However, for sensing the H_2S in living bodies, it is still necessary to develop the COF that can respond to the trace amount of H_2S (HS^- , S^{2-}) in aqueous solution. In 2018, P. Wang et al. reported a COF-based hybrid probe, TpASH-NPHS, for targeting H_2S around the living cells [108]. The hybrid probe was prepared by covalently anchoring a two-photon fluorescent probe 4-amino-1,8-naphthalimide derivative (NPHS) onto an imine-linked COF, TpASH. To further enhance the dispersibility, the micron-sized, bulky TpASH-NPHS was treated by solvent-assisted liquid sonication. The resulting nano-sized TpASH-NPHS can be well dispersed into the aqueous solution. The azide units on NPHS can be reduced to NH_2 in the presence of H_2S (HS^- , S^{2-}), which will increase the fluorescence emission of NPHS. Thus, TpASH-NPHS showed a good performance in two-photon fluorescence imaging of H_2S (HS^- , S^{2-}) in live tumor cells and deep tumor tissues. The hybrid fluorescent probe TpASH-NPHS was able to detect the concentration of H_2S (HS^- , S^{2-}) in the range of 0–20 mM with a LOD of 0.11 mM. Furthermore, TpASH-NPHS was inert to a wide range of interferents, including common anions, biothiols, cysteine, homocysteine, and reactive oxygen species. Notably, since the NPHS was immobilized in the 1D channel of which the diameter is about 1.5 nm, the H_2S (HS^- , S^{2-}) imaging by TpASH-NPHS was not interfered by some intracellular enzymes (diameter > 3 nm), which are also able to reduce the azide group under hypoxic conditions. Hence, this COF-based hybrid probe displayed a great promise in clinical applications.

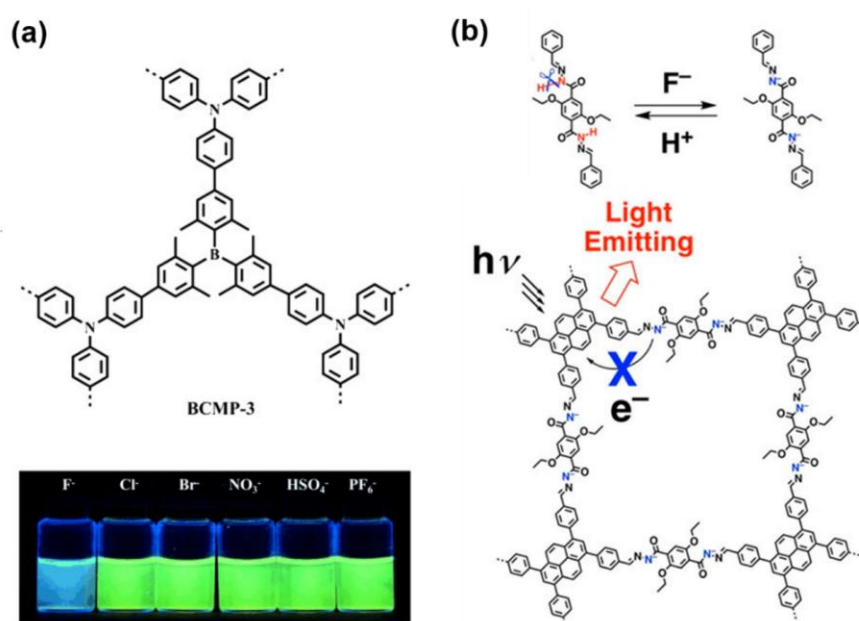


Figure 9. (a) BCMP-3 for F^- sensing [109]. Copyright 2015 John Wiley and Sons; (b) TFPPy-DETHz-COF for F^- sensing [110]. Copyright 2018 American Chemical Society.

3.3. Molecular Sensing

3.3.1. Explosive Sensing

Explosive detection is widely required in the security of airports, railway stations, and border checks. Therefore, plenty of effort has been devoted to the fast, portable detection of explosives. Various COFs that can be used for explosive sensing have been developed (Table 6) [76,111–130].

Table 6. COF-based explosive sensing.

| COF Names | Year | Analyte | Type of Detectable Signal | Detection Range | LOD | Reference |
|-------------------------|------|---|-----------------------------|--|--|-----------|
| SNW-1 | 2012 | picric acid | Fluorescence, "turn off" | 0.2–52.4 μM | 0.05 μM | [111] |
| COP-2 COP-3 COP-4 | 2012 | picric acid TNT | Fluorescence, "turn off" | - | ~1 ppm ~1 ppm | [117] |
| Py-Azine COF | 2013 | picric acid | Fluorescence, "turn off" | 0–70 ppm | - | [116] |
| COF-301 COF-401 | 2015 | picric acid | Fluorescence, "turn off" | - | 1 ppm | [112] |
| iPrTAPB-TFP | 2015 | picric acid | Fluorescence, "turn off" | - | 1 ppm | [118] |
| TfpBDH-CONs | 2015 | picric acid | Fluorescence, "turn on/off" | - | 1×10^{-3} M | [119] |
| TRIPTA | 2016 | picric acid | Fluorescence, "turn off" | - | 51.96 nM | [120] |
| 3D-Py-COF | 2016 | picric acid | Fluorescence, "turn off" | 0–20 ppm | - | [121] |
| 3'PD | 2017 | picric acid triacetone triperoxide | Fluorescence, "turn off" | | | [115] |
| PI-CONs | 2017 | picric acid | Fluorescence, "turn off" | 0.5–10 μM | 0.25 μM | [122] |
| COP-612 COP-616 | 2017 | picric acid | Fluorescence, "turn off" | - | 15 ppm | [113] |
| LMOP-15 | 2017 | picric acid | Fluorescence, "turn off" | - | 0.33 μM | [76] |
| iPrTAPB-Azo-COP | 2018 | picric acid | Fluorescence, "turn off" | - | 13 ppm | [123] |
| 1 | 2018 | picric acid | Fluorescence, "turn off" | - | 68 ppb | [124] |
| CMP-LS1 CMP-LS2 | 2018 | picric acid | Fluorescence, "turn off" | - | - | [125] |
| Py-TPE-COF | 2018 | picric acid | Fluorescence, "turn off" | - | 10 ppm | [126] |
| DL-COF | 2019 | picric acid 2,4-dinitrophenol 2,4-dinitrotoluene 4-nitrophenol 4-nitrotoluene | Fluorescence, "turn off" | - | 13.10 ppb 8.56 ppb 10.40 ppb 5.15 ppb 6.92 ppb | [127] |
| LPCMP1-4 | 2019 | TNT | Fluorescence, "turn off" | 0–100 ppm | - | [128] |
| ANCOF | 2020 | Dichloran 4-nitroaniline | Fluorescence, "turn off" | - - | 142 ppb 89 ppb | [129] |
| A-COF | 2021 | picric acid | Fluorescence, "turn off" | - | 0.09 μM | [114] |
| TFPB-TTA COF | 2022 | DNP picric acid | Fluorescence, "turn off" | 50 nM–10 μM 50 nM–12.5 μM | 18 nM 16 nM | [130] |

Nitroaromatics, the most widely used explosive, have an electron-deficient aromatic ring which is an effective fluorescence quencher. It can be expected that the fluorescence of some COFs can be easily quenched by adsorbed nitroaromatics. Therefore, the key point to realizing COF-based nitroaromatics detection is designing a fluorescent COF that can effectively adsorb nitroaromatics. Early in 2012, L.-G. Qiu and coworkers demonstrated a melamine-based COF (SNW-1) for trace-level detection of nitroaromatic explosives [111]. The melamine-based fluorescent COF was synthesized by the microwave-assisted reaction between terephthalaldehyde and melamine. It was found that the fluorescent emission of SNW-1 can be quenched after adsorbing nitroaromatics due to the transfer of photoexcited electrons from the excited luminescence network donor to the electron-deficient nitroaromatic acceptors. In the THF-water (1:9, *v/v*) mixture, the intensity of

the fluorescence linearly decreased with the concentration of nitroaromatics including nitrobenzene, 4-nitrotoluene, 4-nitrophenol, 2,4-dinitrotoluene (DNT), picric acid, 2,4,6-trinitrotoluene (TNT), and 2,4,6-trinitrophenylmethylnitramine. The LODs for TNT and DNT were $1.51 \times 10^{-6} \text{ mol L}^{-1}$ and $2.8 \times 10^{-6} \text{ mol L}^{-1}$, respectively. Remarkably, the LOD for picric acid can be as low as $5.0 \times 10^{-8} \text{ mol L}^{-1}$ (11.5 ppb). Furthermore, L.-G. Qiu and coworkers also applied SNW-1 to detect the vapor of DNT, which is a volatile by-product of commercial TNT. It can be found that the fluorescence of SNW-1 decreased by 50% within 10 s, suggesting an ultrafast response to DNT. The LOD of SNW-1 for DNT vapor detection was calculated to be 9.8 ppb, much lower than most DNT detectors that had been reported.

In the following years, many COFs of which the fluorescence can be quenched by nitroaromatics were found. For example, D. Jiang and coworkers reported an azine-linked COF, of which the fluorescence can be quenched by some nitroaromatics like picric acid, 2,4-dinitrophenol (DNP), DNT, 2-nitrophenol, and 2-nitrotoluene (Figure 10a) [109]. It can be also found that the quenching result from picric acid was much more significant than other nitroaromatics. The authors demonstrated the strong quenching effect can be attributed to the hydrogen bond formed by the -OH group of the analytes and the open N atoms on the COF skeleton. In addition, the three nitro groups of picric acid resulted in the most deficient π system for driving the fluorescence quenching and the strongest hydrogen bond with the azine for promoting the quenching process. After the reveal of the mechanism, many COFs for picric acid detections were successfully designed and synthesized [112–126,129,130]. The LOD has been decreased to $\sim 10 \text{ nM}$ (Table 6). Furthermore, the interference from other nitroaromatics especially dinitrophenol and nitrophenol has been reduced to the largest extent [112–114]. Moreover, considering that other nitroaromatics including dinitrophenol and nitrophenol are also explosive, it can still be concluded that the fluorescence quenching strategy based on COFs is an effective method for the nitroaromatic explosive initial inspection.

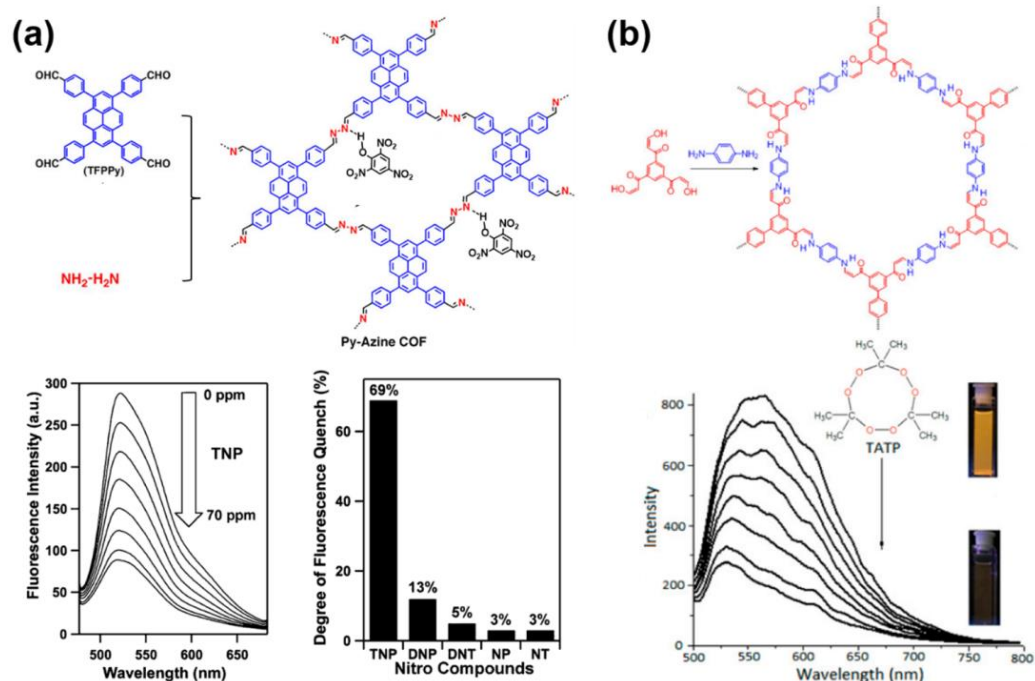


Figure 10. (a) The azine-linked COF for picric acid (2,4,6-trinitrophenol) detection. 2,4,6-trinitrophenol (TNP), 2,4-dinitrophenol (DNP), 2,4-dinitrotoluene (DNT), 2-nitrophenol (NP), and 2-nitrotoluene (NT) [116]. Copyright 2013 American Chemical Society; (b) The COF for TATP sensing [115]. Copyright 2017 American Chemical Society.

In addition, the COF-based detection of non-nitroaromatic explosives has been also presented. In 2018, D. F. Perepichka synthesized two kinds of fluorescent COFs (3BD and 3'PD) via Michael Addition–Elimination [115]. The fluorescence of the two COFs cannot only be quenched by nitroaromatics like picric acid but is also sensitive to triacetone triperoxide (TATP), which is another well-known explosive. The quenching caused by TATP was possibly attributed to the oxidation of the enamine moieties in 3BD and 3'PD (Figure 10b). A total of 1 μM TATP solved in CH_2Cl_2 can be detected. The authors suggested that the quench should not result from the oxidation of the enamine moiety in the COF skeleton rather than the electron transfer from excited COFs to the analyte, like nitroaromatics.

3.3.2. Iodine Sensing

Radioiodine (^{129}I and ^{131}I), which is generated by nuclear fission, is an important index for detecting nuclear fallout. It is pernicious to the human body because of its long radioactive half-life (^{129}I , 1.57×10^7 years) [131] and high volatility. Therefore, it is widely concerned to detect radioiodine fast and sensitively. COF and its analogs have been proved to be excellent adsorbents for iodine removal. For example, TPB–DMTP–COF synthesized by D. L. Jiang and coworkers can effectively adsorb I_2 vapor with an adsorption capacity of 6.2 g/g [132]. As with nitroaromatics, the molecule of iodine is an electron-deficient species. The charge transfer from the electron-rich COF skeleton to the iodine can significantly quench the fluorescence of the COF. Thus, it is very likely to achieve “turn off” fluorescence sensing to iodine by COF or its analogs. Recently, a number of iodine sensors based on COPs was presented [133–139]. In 2020, T. M. Geng et al. prepared a fluorescent covalent triazine-based framework (TDPDB) by Friedel–Crafts polymerization reaction of N, N'-diphenyl-N, N'-di(m-tolyl)benzidine (DPDB) with 2,4,6-trichloro-1,3,5-triazine (TCT) [140]. It exhibited an excellent capacity for capturing iodine (3.93 g/g). In the meantime, the adsorption of iodine quenched the fluorescence of TDPDB remarkably. The quenching coefficient (K_{sv}) was measured as $5.83 \times 10^4 \text{ L mol}^{-1}$ and the LOD reached 2.57 μM . It indicated that TDPDB can be used for highly sensitive I_2 detection. Furthermore, the concentration of PA can be also measured by TDPDB based on the same mechanism. The K_{sv} and LOD for PA detection were determined as $1.55 \times 10^4 \text{ L mol}^{-1}$ and 19.3 μM , respectively. The next year, Y. X. Zhao et al. reported a COF (COF-PA) with acetylene groups in its 1D channels [131]. The acetylene groups greatly accelerated the adsorption rate of I_2 vapor. The charge transfer between COF-PA and I_2 effectively decreased the intensity of the fluorescence of COF-PA. I_2 at ppm level in THF solution can be well detected by the fluorescence quenching of COF-PA.

3.3.3. Drug Sensing

Drug sensing has a strong practical value and significance because it is a key essential step in investigating pharmacokinetics, which is quite instructive in clinical treatment. Moreover, the drug residue, especially the antibiotics' residue, in food and drinkable water because of the abuse of drugs was frequently reported in recent decades. It is likely to result in the appearance of the “superbug” by which the infection caused is incurable because it is resistant to the existing antibiotics. Hence, the fast detection of drugs, especially antibiotics, in bodily fluids, food, drink, and environment attracted increasing attention. COF-based detections of drugs, especially various antibiotics [49,107,140–153] were frequently reported in recent years, especially in the past five years. Notably, as shown in Table 7, it can be found that, unlike gases or ions, most of the COF-based drug detection is accomplished by a hybrid material containing COFs, rather than by a separate COF, because most of the binding sites for the selective capture of the drug molecules, including aptamers, metal ions and so on, were difficult to be robustly pre-immobilized onto the monomers. They are easy to detach from the monomers or be damaged during the solvothermal synthesis of COFs. Hence, they can only be introduced by the “post-functionalization” of the COFs. In addition, in some COF-based sensors for drug detection, the selective capture of drug

molecules was not always achieved by the COFs, but by other materials like molecular imprinting membranes.

Tetracycline, a broad-spectrum antibiotic, is widely used in the treatment of bacterial infections in humans and animals. Therefore, tetracycline residues were frequently found in the products of the breeding industry or aquaculture. Thus, as shown in Figure 11a, X. H. Ma synthesized a Zr-coordinated amide porphyrin-based COF by a liquid-liquid interface method [144]. The COF exhibited strong catalytic effects and high electrical conductivity. Hence it was immobilized onto a GCE via the polymerization of the *o*-phenylenediamine to yield an electrochemiluminescence (ECL) sensor. In the meantime, molecular imprinting technology was used to enhance the selectivity of tetracycline. It was found that the intensity of the ECL signal obtained using a luminol-H₂O₂ system linearly increased with the concentration of tetracycline. The linear range was 5–60 pM and the LOD was calculated as 2.3 pM. In 2021, Y. S. Zhang reported a COF-containing porous hybrid, Mg@Fe-MIL-101/TpPa-1-COF, grown on stainless steel mesh (Figure 11b) [152]. The porous property of Mg@Fe-MIL-101 exposed more catalytical active sites, and the hybrid structure facilitated the electrons' migration. Therefore, the Mg@Fe-MIL-101/TpPa-1-COF exhibited excellent photocatalytic tetracycline degradation capacity. Meanwhile, the Mg²⁺ in the hybrid can coordinate with tetracycline and form the fluorescent Mg-tetracycline complex. Hence, fluorescent detection can be realized simultaneously with photocatalytic tetracycline removal (Figure 11b).

Table 7. COF-based detection of drugs, insecticides and spices.

| Year | COF/COF Hybrid Names | Analyte | Specific Binding Site | Type of Detectable Signal | Detection Range | LOD | Reference |
|------|--|----------------------------|-------------------------------------|-------------------------------------|---|--|-----------|
| 2018 | TAPB–DMTTAPB–DMTP–COFs/AuNPs | Chlorogenic acid | - | Electrochemical signals (CV) | 1.0×10^{-8} – 4.0×10^{-5} mol L ⁻¹ | 9.5×10^{-9} mol L ⁻¹ | [140] |
| 2018 | 2D Fe–CTFs | Sarcosine ochratoxin A | Sarcosine oxidase Aptamer | Chromism | 10–100 μ M 0.2–0.8 μ M | 0.56 μ M - | [107] |
| 2019 | Py–M–COF | Enrofloxacin Ampicillin | Aptamer | Electrochemical signals (EIS) | 0.01 pg mL ⁻¹ –2 ng mL ⁻¹ 0.001–1000 pg mL ⁻¹ | 6.07 fg mL ⁻¹ 0.04 fg mL ⁻¹ | [49] |
| 2019 | QD–grafted COFs | Ferulic Acid | Molecular imprinting, amino groups | Fluorescence, “turn on” | 0.03–60 mg kg ⁻¹ | 5 μ g kg ⁻¹ | [141] |
| 2019 | MIP/MoS ₂ /NH ₂ –MWCNT@COF | Sulfamerazine | Molecular imprinting | Electrochemical signals | 0.30 – 2.0×10^2 μ M | 0.11 μ M | [142] |
| 2019 | Ce–MOF@MCA | Oxytetracycline | Aptamer | Electrochemical signal (EIS) | 0.1–0.5 ng mL ⁻¹ | 17.4 fg/mL | [143] |
| 2019 | Zr–amide–Por-based 2D COF | Tetracycline | Molecular imprinting | Electrochemical signals | 5–60 pM | 2.3 pM | [144] |
| 2019 | Eu@TpPa–1 | Levofloxacin | Europium ions | Fluorescence, “turn off” | 10^{-6} – 10^{-2} M | 0.2 μ M | [145] |
| 2019 | MIOP based on QDs–grafted COFs | Tyramine | H-bond, shape selectivity | Fluorescence, “turn on” SPE–HPLC | 35–35,000 μ g/kg 20–2000 μ g/kg | 7.0 μ g/kg 5.0 μ g/kg | [146] |
| 2019 | NUS–30 | L-dopa | Azine | Fluorescence, “turn off” | | | [147] |
| 2019 | PATP@AuNPs–crosslinked MIP | Dopamine | Molecular imprinting | electrochemiluminescence | 10^{-14} – 10^{-6} M | 2×10^{-15} M | [148] |
| 2020 | UiO–66–NH ₂ /MCA/MWCNT@rGONR | Kanamycin | Aptamer | Electrochemical signals | 25–900 nM | 13 nM | [149] |
| 2020 | TpPa–1@Dye | Sialic acid | Cr ³⁺ | Fluorescence, “turn on” | 10^{-8} – 10^{-2} M | 7.08×10^{-9} M | [150] |
| 2021 | Au@COF/GO–NH ₂ | Chloramphenicol | Aptamer | Electrochemical signal (EIS) | 0.0001–1 ng mL ⁻¹ | 16.13 fg mL ⁻¹ | [151] |
| 2021 | Mg@Fe–MIL–101/TpPa–1–COF | Tetracycline | Mg ²⁺ | Fluorescence, “turn off” | - | - | [152] |
| 2021 | COF–1 or COF–2 | Tetracycline ofloxacin | - | Fluorescence, “turn off” | 0.005–0.0625 mM 0.025–0.25 mM | 0.002 mM 0.0065 mM | [153] |
| 2021 | Eu@TpPa–1 | 5-Fluorouracil | π – π stacking interactions | Fluorescence | 10^{-7} – 10^{-3} M | 6.45×10^{-8} M | [154] |

Table 7. Cont.

| Year | COF/COF Hybrid Names | Analyte | Specific Binding Site | Type of Detectable Signal | Detection Range | LOD | Reference |
|------|----------------------|---|---|---------------------------|--|--|-----------|
| 2018 | DAAQ–TFP | Diflubenzuron Triflumuron Hexaflumuron Teflubenzuron | Amino and carbonyl group (H bonding) π – π stacking interactions | HPLC | 0.2–160.0 ng mL ⁻¹ 0.2–160.0 ng mL ⁻¹ 0.2–160.0 ng mL ⁻¹ 0.2–160.0 ng mL ⁻¹ | 0.02 ng mL ⁻¹ 0.02 ng mL ⁻¹ 0.05 ng mL ⁻¹ 0.04 ng mL ⁻¹ | [155] |
| 2019 | NH ₂ @COF | Carboxylic acid pesticides | Amino group | HPLC-DAD | 0.2–100 ng mL ⁻¹ | 0.04–0.20 ng mL ⁻¹ | [156] |
| 2019 | CNs–grafted COFs@MIP | 4-ethylguaiacol | The surface of the silica matrix by acid–base pairing interactions | Fluorescence, “turn off” | 0.025–1 μ g mL ⁻¹ | 17 ng mL ⁻¹ | [157] |

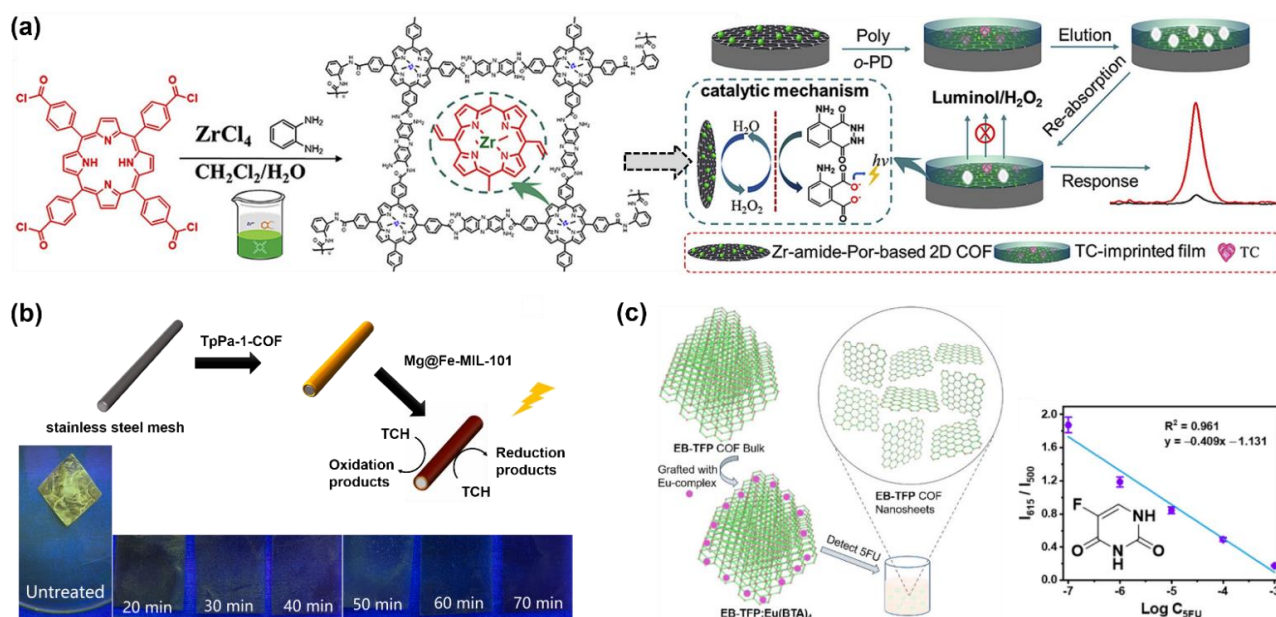


Figure 11. (a) Zr-coordinated amide porphyrin-based COF for tetracycline detection with the aid of molecular imprinting technology [144]. Copyright 2019 Elsevier B.V.; (b) The preparation of Mg@Fe–MIL–101/TpPa–1–COF, and its fluorescent detection of tetracycline realized simultaneously with photocatalytic tetracycline removal [152]. Copyright 2021 Elsevier B.V.; (c) EB-TFP:Eu(BTA)₄ for the detection of 5-Fluorouracil [154]. Copyright 2021 American Chemical Society.

Due to the side effects and increasing resistance, the use of antibiotics in the clinic treatment is being updated, therefore, the COF-based antibiotic detection needs to be constantly extended. B. Yan and coworkers prepared a Eu³⁺ functionalized COF hybrid material (Eu@TpPa–1) by simply soaking TpPa-1 COF [158] in a EuCl₃ solution [145]. It was found that due to the coordination between Eu³⁺ and levofloxacin, Eu@TpPa–1 can act as a fluorescence sensor toward levofloxacin with a turn-on response. The linear range of the levofloxacin sensing was 1–10⁴ μM, and the LOD was calculated as 0.2 μM. The sensor also displayed a fast response to levofloxacin which was less than 1 min. In the meantime, it also exhibited a good selectivity refraining from the interference of other components in serum and urine. In 2021, S. Wang reported a polyimide COF of which fluorescence can be quenched by levofloxacin, tetracycline, and some metal ions [153]. It exhibited a potential application in the fast identification of multiple harmful substances in drinkable water.

In addition to antibiotics, COF-based sensing of other drugs was also reported (Table 7). For example, 5-fluorouracil (5FU), an anticancer drug, can be detected by a COF hybrid material (EB-TFP:Eu(BTA)₄) prepared by B. Yan et al. (Figure 11c) [154]. The hybrid material was prepared by soaking a previously reported COF [159] in an Eu complex. The adsorption of 5FU can disturb the π–π stacking interaction between the 2D sheets of EB-TFP:Eu(BTA)₄, leading to the change in the fluorescent spectra. It resulted in an increase in the fluorescent peak at 615 nm and an decrease in the peak at 500 nm. The intensity ratio I_{615}/I_{500} linearly decreased with the logarithm of the concentration of 5FU. Therefore, a 5FU sensing based on fluorescence can be achieved. The linear detection range of the 5FU sensing was 10⁻⁷–10⁻³ M. The calculated LOD was 5.13 × 10⁻⁸ M. In addition, B. Yan et al. demonstrated a dye-functionalized COF for ultrasensitive monitoring of sialic acid, which is a widely-used cosmetic additive and biomarker of ovarian cancer. Similar to the above-mentioned Eu@TpPa–1, B. Yan et al. loaded fluorescein sodium (TpPa–1@Dye) into the porous TpPa-1 COF [154]. The TpPa–1@Dye was mixed in sodium alginate solution and finally formed a hydrogel with the assistance of Cr³⁺. The interaction between TpPa–1@Dye and Cr³⁺ caused fluorescence quenching of fluorescein, while the sialic acid

can take away Cr^{3+} from the TpPa-1@Dye leading to the recovery of the fluorescence. The fluorescence recovery is fast and very sensitive to the addition of sialic acid, the LOD of the sialic acid detection in serum by this approach can be as low as 8.71×10^{-9} M.

3.3.4. Small Biomolecules Sensing

The level of some small biomolecules, including glucose, uric acid, Glutathione (GSH), et al., are key marks of some serious diseases. Hence the detection of them is very important in the healthcare and clinic diagnosis. Recently, with the demands for portable and wearable healthcare devices, the reports on new materials for facile detection of the above small biomolecules have been increasing. Recently, some COFs or COF-based hybrid materials were designed and synthesized for detecting glucose, uric acids, GSH, and other small biomolecules (Table 8) [26,27,102,160–163].

Table 8. COFs or COF-based hybrid materials for detecting glucose, uric acids, GSH, and other small biomolecules.

| Analyte | Year | COF/COF Hybrid Names | Specific Binding Site | Type of Detectable Signal | Detection Range | LOD | Reference |
|---------------|------|-------------------------|-----------------------|---------------------------|--|---------------------|-----------|
| Glucose | 2018 | Fe-COF | Glucose oxidase | Chromism | 5–350 μM | 1.1 μM | [160] |
| | 2019 | COF _{DHTA-TTA} | Glucose oxidase | Electrochemical signal | 0.60 μM –6.0 mM | 0.38 μM | [102] |
| | 2020 | Fe-PorCOF | Glucose oxidase | Chemiluminescence | 0.01–10 μM | 5.3 nM | [161] |
| | 2021 | COFHD-GOX | Glucose oxidase | Chromism | 5–2000 μM | 0.54 μM | [162] |
| Uric acid | 2021 | COF-DC-8 | Hydroxyl, triazine | Electrochemical signals | 5.0–25 μM , 25–250 μM | 0.77 μM | [163] |
| Ascorbic acid | 2021 | COF-DC-8 | Hydroxyl, triazine | Electrochemical signals | 30–180 μM , 0.18–1.5 μM | 12.0 μM | [163] |
| Dopamine | 2021 | COF-DC-8 | Hydroxyl, triazine | Electrochemical signals | 1.0–6.0 μM , 8.0–50 μM | 0.25 μM | [163] |
| GSH | 2020 | COF-300-AR | | Chromism | 1–15 μM | 1.0 μM | [26] |
| | 2021 | Py-TT COF | | Chromism | 0.4 – 60 μM | 0.225 μM | [27] |

The concentration of glucose in blood is an essential index for the diagnosis of diabetes. Plenty of methods to detect the concentration of glucose have been developed. The basic strategy to sense glucose is by detecting H_2O_2 yielded by the enzymic oxidation of glucose. In 2018, J. N. Wang et al. and co-workers prepared a Fe-porphyrin-based peroxidase-mimicking COF (Fe-COF) [160]. Like the COF demonstrated by J. D. Qiu and coworkers [148], Fe-COF can be used to quantitatively detect the $[\text{H}_2\text{O}_2]$ by the generation of the oxTMP with blue color. Furthermore, upon the mixing of glucose oxidase (GOx), the combination of the enzymic glucose oxidation and Fe-COF-catalyzed oxTMP production resulted in the realization of a glucose sensor. The detection range of the sensor was from 5 to 350 μM . The detection limit was 1.0 μM . On the basis of this principle, several COF-based glucose sensors with improved properties were developed [102,161,162]. For example, the function of the pH sensor mentioned above by L. Wang and coworker can be extended for glucose sensing [102]. Recently, J.-Yu Yue et al. prepared a glucose sensor by coupling the GOx on a carboxyl-containing COF via a covalent amide bond [162]. The sensor showed good recoverability and storage stability. Even after 100 days of storage, the relative activity of GOx was still more than 85%. In the meantime, this sensor displayed a wider linear range from 0.005 to 2 mM and a lower LOD which was calculated as 0.54 mM.

The level of uric acid in serum is the most important index for the diagnosis of gout, which is a common ailment in developed countries. In 2021, Y. S. He et al. developed a COF-based electrochemical sensor for detecting uric acid [163]. For fabricating the sensor, a poly-fuchsin basic film was fabricated on the surface of a bare glass GCE. Then Au nanoparticles were doped on a carboxylated COF (ACOF-TaTp), yielding a hybrid, AuNPs@ACOF-TaTp.

Finally, the sensor was achieved by dropping the hybrid on the poly-fuchsin basic coated GCE. The COF in the sensor provided a high surface area and numerous binding sites (H-bond binding) for the analyte. The existence of AuNPs enhanced the conductivity, while the poly-fuchsin basic film can accelerate the electron transfer process. Therefore, the sensor exhibited high affinity to the analyte and high sensitivity and selectivity in uric acid sensing. It was reported that there were two linear response ranges of the AuNPs@ACOF-TaTp-based uric acid sensor, 5.0–25 μM , and 25–250 μM . The LOD was calculated as 0.77 μM , (normal uric acid level of human: 89–416 μM) indicating the sensor has the potential to be used in the detection of uric acid in serum. In addition, the sensor can be applied to detect the concentrations of ascorbic acid and dopamine, which are also important biomolecules.

GSH is a biomolecule that widely exists in all kinds of cells in the human body. The excessive glutathione in serum usually suggests hepatocellular injury or tumor. In 2020, H. L. Chen and coworkers reported an amine-linked COF (COF-300-AR) obtained by reducing the corresponding imine-linked COF (COF-300) (Figure 12a) [26]. It exhibited excellent oxidase-mimicking activity under light irradiation of which $\lambda = 400 \text{ nm}$, catalyzing the oxidation of TMB by the formation of reactive oxygen species like $\bullet\text{OH}$ and $\text{O}_2^{\bullet-}$ free radicals in the presence of dissolved oxygen. However, the reducibility of GSH can prevent the oxidation of TMB and lighten the blue color resulting from oxTMB. Therefore, the concentration of glutathione can be measured by colorimetric analysis. The authors successfully applied COF-300-AR to detect GSH levels in HL60 cells. It displayed good selectivity and high sensitivity. Similarly, Z. Lin et al. synthesized a COF (Py-TT COF) using the condensation between tetrakis(4-aminophenyl)pyrene (Py), which can act as an electron donor, and thieno[3,2-*b*]thiophene-2,5-dicarbaldehyde (TT), which can act as an electron acceptor (Figure 12b) [27]. Like COF-300-AR, Py-TT COF exhibited superior enzymatic catalytic activity, which could catalyze the oxidation of TMB by the formation of ROS under visible light irradiation. Therefore, based on the similar mechanism, the concentration of GSH can be determined by the decrease of the blue color generated by oxTMB. The linear range of this approach was 0.4 – 60 μM , and the LOD was 0.225 μM , satisfying the detection of the GSH in human serum.

3.3.5. Other Small Molecules Sensing

Besides the residue of antibiotics, the detection of insecticides residual is also an important problem in agriculture [155,156]. For insecticide sensing, Y. H. Song et al. synthesized a COF by the imine condensation (DAAQ-TFP) between 2,6-diaminoanthraquinone (DAAQ) and 1,3,5-triformylphloroglucinol (TFP) [155]. DAAQ-TFP exhibited a very good capacity for adsorbing benzoylurea insecticides due to the hydrogen bond and π - π interaction between the benzoylurea and COF skeleton. The benzoylurea insecticides adsorbed by DAAQ-TFP can be eluted by organic solvent for quantitative detection by HPLC. This approach can be applied for detecting insecticide residuals in fruit samples and provided very low detection limits ($\sim 0.1 \text{ ng mL}^{-1}$).

The COF-based detection of spice, of which concentration is quite important in the food industry, was also investigated. H. L. Liu and co-workers reported a fluorescent nanoprobe (CN-grafted COF@MIPs) for the detection of 4-ethylguaiaicol, which is a crucial index to evaluate the quality of some kinds of wine [157]. The probe was a 4-ethylguaiaicol imprinted polymer doped with a COF grafted onto carbon nanodots. The molecular imprinting and $-\text{NH}_2$ in the hybrid material enhanced the selective uptake of the analyte. The adsorption of 4-ethylguaiaicol quenched the fluorescence of carbon nanodots through charge transfer interaction. Under optimized conditions, the fluorescence of CN-grafted COF@MIPs drops linearly as the concentrations of 4-ethylguaiaicol increase from 0.025 to 1 $\mu\text{g mL}^{-1}$, with a LOD of 17 ng mL^{-1} .

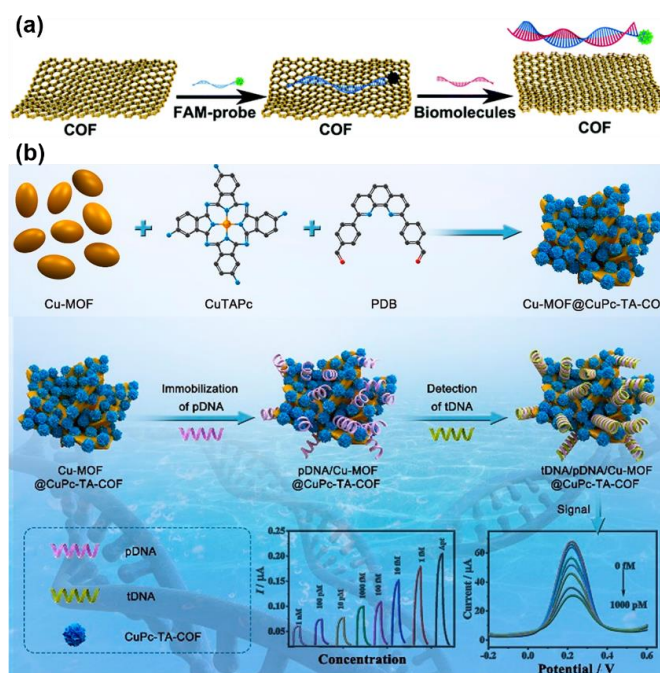


Figure 12. (a) COF–300–AR for GSH detection [26]. Copyright 2020 American Chemical Society; (b) Py–TT COF for GSH sensing [27]. Copyright 2021 American Chemical Society.

Finally, it is worth mentioning that Y. Cui and co-workers reported a chiral 1,1'-bi-2-naphthol-based (BINOL-based) COF for sensing chiral organic compounds [164]. The COF was synthesized by imine condensations of tetrakis(4-aminophenyl)ethene (TPE-TAM) and the chiral linker (R or S) 6,6'-dichloro-2,2'-diethoxy-1,1'-binaphthyl-4,4'-dialdehyde (BINOL-DA). The chiral linker created a 1D channel with high enantioselectivity for the discriminating uptake of chiral analytes. For example, the nanosheets of the COF synthesized by (R)-BINOL-DA can adsorb more (–)- α -pinene than (+)- α -pinene. Thus, the (–)- α -pinene can result in a faster and greater fluorescence quench than (+)- α -pinene at the same concentration. The authors found that the BINOL-based COF nanosheets exhibited much better selectivity and enantio-sensitivity to other BINOL-based sensing systems, probably due to the steric confinement of the COF channels and conformational rigidity of the immobilized BINOL groups.

3.3.6. Biomacromolecule Sensing

Biomacromolecules, including polysaccharides, proteins, nucleic acids, et al., are essential components of living organisms and play an important role in various life activities. The detection of biomacromolecules, especially proteins and nucleic acids, is extensively needed in clinical treatment, public health, and environmental protection. Recently, a number of COFs or COF-containing hybrid materials have been developed for sensing proteins and nucleic acids (Table 9).

Although protein is a kind of biomacromolecule with huge diversity, it is not difficult to specifically enrich the target protein from the sample solution, because most proteins can be recognized and captured by the corresponding antibody. Due to the large specific surface area, COFs are good carriers for immobilizing the antibodies. Moreover, other functional species can be simultaneously introduced onto the COF sheets to produce a detectable signal after the target protein was bound via antigen-antibody recognition. Based on this strategy, some COF-containing sensors for detecting protein with diagnostic significance were developed recently [165–169].

In 2018, T. Zhang et al. reported a COF-based immunosensor for detecting cardiac troponin I (cTnI), which is an important marker for angina pectoris and myocardial infarction (Figure 13a) [165]. Firstly, AuNPs were loaded into the pore of a previously-

reported COF [170], then cTnI secondary antibody (Ab_2 -cTnI) was immobilized onto the AuNPs. Finally, toluidine blue (TB) was loaded into the COF, yielding a COF-based label, TB-Au-COFs- Ab_2 . Meanwhile, a GCE was coated by TiO_2 NPs which is successively modified by polypyrrole, AuNPs, and cTnI primary antibody (Ab_1 -cTnI). By the specific recognition antigen-antibody, the TB-Au-COFs- Ab_2 , analyte, and modified GCE can form a sandwich-like structure, resulting in a redox signal that can be detected by square-wave voltammetry. The concentration of cTnI can be determined by the intensity of the square-wave voltammetric signal. The authors found that the AuNP-doped COF can amplify the electrochemical signal and enhance the performance of the immunosensor. The immunosensor showed a linear range from 0.5 pg mL^{-1} to 10.0 ng mL^{-1} and a low detection limit of 0.17 pg mL^{-1} . In 2021, S. N. Feng et al. reported a similar approach to detect cTnI [166] (Figure 13b). TB in the above work was replaced by horseradish peroxidase (HRP) to fabricate the COF-based label. Meanwhile, Ab_1 -cTnI was modified directly on a gold electrode instead of GCE, avoiding the complex modification procedure. After the formation of the antibody-antigen-antibody sandwich structure, H_2O_2 and hydroquinone was added, and the intensity of the redox signal of hydroquinone can be detected by cyclic voltammetry and used to determine the concentration of cTnI.

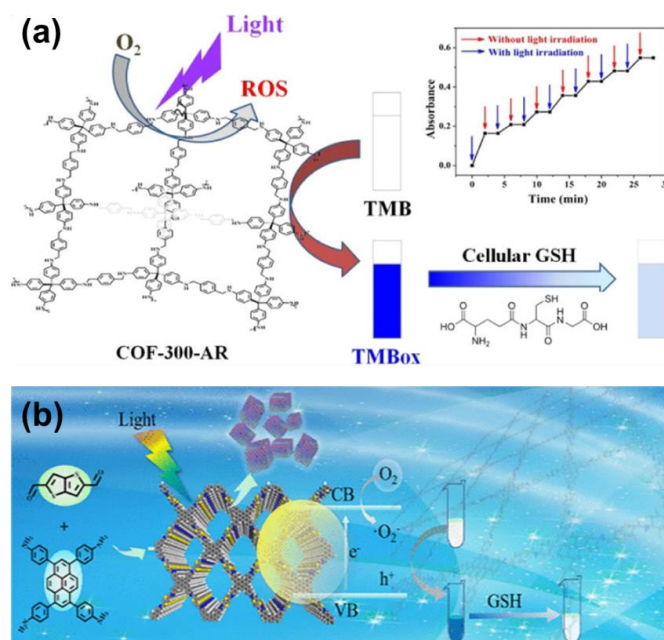


Figure 13. (a) Immunosensor for cTnI Detection based on TB-Au-COFs- Ab_2 [165]. Copyright 2018 Elsevier B.V; (b) Immunosensor for cTnI Detection based on HRP- Ab_2 -Au-COF [166]. Copyright 2021 American Chemical Society.

X. Fang and coworkers prepared a COF-coated Fe_3O_4 NPs as an immunoaffinity probe for the detection of heat shock protein 90α (Hsp90 α), a biomarker for liver cancer [167]. The probe was prepared by in situ growth of COFs on an $-NH_2$ coated Fe_3O_4 NPs, and successively modified by Hsp90 α antibody and PEG. The probe can selectively capture Hsp90 α in the sample and be collected by the magic field. The Hsp90 α on the probe was digested with free trypsin and the resulting peptides' mixture can be collected for further MALDI-TOF-MS analysis to determine the existence of Hsp90 α .

Nucleic acid is an essential biomacromolecule in living bodies and the carrier of genetic information. Nucleic acid detection is widely applied in the identification of bacteria and viruses. During the pandemic caused by COVID-19, nucleic acid detection played a huge part in tracking the virus and preventing the spread of the disease. The key feature of nucleic acid is the base pairing. It allows the detection of a particular nucleic acid segment

by using its complementary sequence. Based on this principle, some COF-based detection of DNA was developed [28,171–173].

In 2017, X.-P. Yan demonstrated a versatile COF-based platform for sensing DNA. The sensor is on the basis of the recognition of the complementary DNA sequences and fluorescent quenching (Figure 14a). For detecting a particular DNA sequence (target DNA), its complementary sequence modified with a carboxyfluorescein (FAM) label was adsorbed onto a COF (TpTta) [171] containing triazine, amino- and carbonyl-group via hydrogen bonding, and π - π interaction. The adsorption of the FAM-labeled complementary sequence led to the quench of the fluorescence. However, the hybridization between the target DNA and the FAM-labeled complementary sequence led to the formation of double-stranded DNA that can detach from TpTta, resulting in the fluorescent recovery of the carboxyfluorescein. Moreover, the author found that quantitatively ATP detection can be also achieved by replacing the above FAM-labeled complementary sequence with the FAM-labeled adenosine 5'-triphosphate (ATP) aptamer probe. The enhanced fluorescence intensity showed a good linear relationship with the ATP concentration in the concentration range of 25–200 μ M and good selectivity.

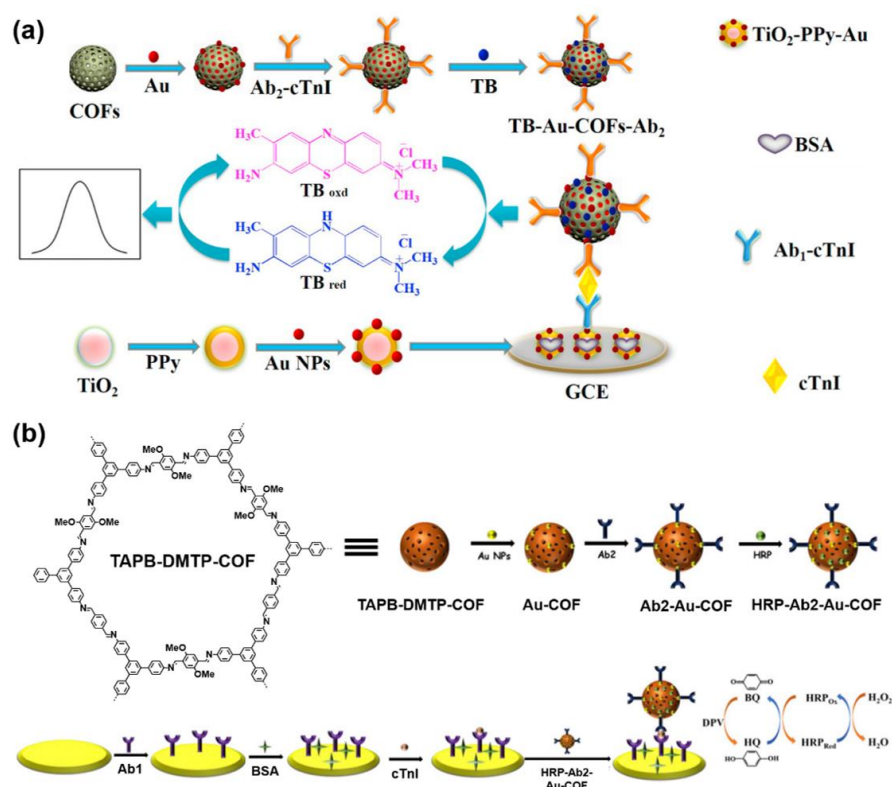


Figure 14. (a) A versatile COF-based platform for sensing DNA [171]. Copyright 2017 Royal Society of Chemistry; (b) MOF@COF Heterostructure Hybrid for Dual-Mode Photoelectrochemical–Electrochemical HIV-1 DNA Sensing [173]. Copyright 2021 American Chemical Society.

M. R. Xu et al. developed a novel MOF@COF hybrid with excellent electrochemical activity and high photoactivity (Figure 14b) [28]. By immobilizing the complementary sequence, the MOF@COF hybrid can be applied for HIV-1 DNA detection, because the complementary hybridization enhanced the impedance of the hybrid and decreased both the photoelectrochemical and electrochemical currents. Hence, it is possible to achieve a dual-mode detection of HIV-1 DNA in human serum. It was found that both the currents decreased linearly with the increasing \lg [HIV-1 DNA], in the range from 1 fM to 1 nM, and the LODs were calculated as 0.07 and 0.18 fM for PEC and DPV techniques, respectively, indicating that the ultra-sensitive sensing of HIV-1 DNA was realized.

Table 9. COF-based sensing of some typical biomacromolecules.

| Analyte | Year | COF/COF Hybrid Names | Specific Binding Site | Type of Detectable Signal | Detection Range | LOD | Reference |
|--------------------------------|------|---|-----------------------|---|----------------------|--------------------|-----------|
| Cardiac Troponin I | 2018 | TB–Au–COFs–Ab ₂ | Antibody | Chromism | 0.5 pg/mL–10.0 ng/mL | 0.17 pg/mL | [165] |
| | 2021 | HRP–Ab ₂ –Au–COF | Antibody | Chromism | 5 pg/mL–10 ng/mL | 1.7 pg/mL | [166] |
| Heat shock protein 90 α | 2019 | Fe ₃ O ₄ @TpBD–DSS–Ab–MEG | Antibody | MS | | 50 pg/mL | [167] |
| C-reactive protein | 2018 | AuNPs @COF–TPPa-1 | Antibody | Electrochemical signal (EIS, CV) | 0.017 ng/mL | 0.05–80 ng/mL | [168] |
| | 2018 | COF–LZU8 | Antibody | Electrochemical signal (DPV) | 0.016 ng/mL | 0.05–150 ng/mL | [169] |
| | 2019 | p–COF | Aptamer | Photoelectrochemical signal | 0.1 ng/mL | 0.5–100 ng/mL | [174] |
| DNA | 2017 | TpTta | DNA hybridization | Fluorescence, “turn on” | 10–100 nM | 3.7 nM | [171] |
| | 2017 | TPA–COF | DNA hybridization | Fluorescence, “turn on” | 0.02–5 nM | 20 pM | [172] |
| | 2018 | EB-TFP iCOF | DNA hybridization | Fluorescence, “turn on” | 0–32 mM | - | [173] |
| | 2021 | Cu–MOF@CuPc–TA–COF | DNA hybridization | Electrochemical signal Photoelectrochemical signal | 1 fM–1 nM | 0.18 fM 0.07 fM | [28] |

4. Challenges and Future Perspectives

In this review, we discussed the basic principles of COF-based chemical and biological sensing, then demonstrated the application of COFs in the detection of a large number of analytes, including corrosive and harmful gases, water vapor (humidity), ions, explosives, drugs, biomolecules, et al. It can be found that COFs exhibited many advantages in chemical and biological sensing. Firstly, due to the designable structure and easily modified properties, the molecular structure and function of the COFs can be easily extended. There is always a good possibility of designing and synthesizing a COF with a specific function. Hence, a wide range of chemicals and biomolecules can be selectively detected by COFs or COF-based hybrid materials. Secondly, the porous structure of the COFs greatly benefits the enrichment of the analyte, significantly enhancing the sensitivity of the detection. Furthermore, the binding site that can selectively interact with the analyte can be easily linked to the COFs. It will remarkably enhance the selectivity of the sensing. Thus, it can be seen that COFs are good candidates for realizing highly sensitive and selective sensing. Thirdly, diverse aromatic structures endow the COFs with rich optical and electrical properties. Moreover, the unique nature of the COFs allows the COFs to play multiple roles in the chemical and biological sensors, including an analyte concentrator, signal generator, and functional particles' carrier. It will significantly decrease the complexity of the sensing devices.

The above advantages exhibited that COFs are a class of promising materials for chemical and biological sensing. Although great progress has been made, COF-based sensors are still under investigation in the laboratory. However, there are still some remaining disadvantages that inhibit the COF-based sensors from practical application. They will be the important challenges to promoting the utilization of the COF-based sensors. The first challenge is the mass production of the COFs. The monomers for preparing functional COFs need to be obtained by organic synthesis. The complex synthetic route may significantly decrease the yield of the final products, and enhance the cost of COFs production. Furthermore, the method to control the polymerization of the monomers and the crystallization process during the COFs formation is still far from perfect. Obtaining COFs with uniform quality is still difficult to guarantee. Secondly, the most widely used technique for COFs synthesis is the solvothermal method. Therefore, most COFs are obtained as a powder. However, for sensor fabrication, the thin film can exhibit much better performance than the powder due to its uniformity and compactness. Therefore, effective approaches to preparing COFs thin films on various substrates are still eagerly expected. Thirdly, with the development of wearable and implantable sensing devices, the demand for materials with good biocompatibility is increasing. However, the data on the biocompatibility of reported COFs are still deficient. It may limit the further application of COFs in biosensing. COF materials with biocompatibility and biosafety should be developed for promoting its application in domestic, wearable, and implantable sensing devices.

In recent years, substantial efforts have been devoted to creating new COFs with various functions. The increasing number of new COFs will continue to promote its application in the development of chemical and biological sensors. Although the COF-based sensors have been utilized for detecting various analytes, it can still be expected that the emergence of new COFs can further extend the range of the analytes. The selectivity and sensitivity will be further improved. Moreover, with the growing demand for fast and real-time detection of pollutants, dangerous articles, and physiological indexes. Portable, wearable, or even implantable sensors is drawing increasing attention. As mentioned above, COFs are usually able to play multiple roles in a sensor, for example, being an analyte concentrator and signal generator simultaneously. It can remarkably reduce the size and complexity of the sensor. Therefore, COFs also display great potential in constructing miniaturized sensing devices. Additionally, it is also promising to develop COF-based sensors which are suitable to work in special environments, such as the polar region, space environment, and body fluids. Thanks to the increasing eagerness for environmental

protection, security, food safety, and healthcare, developing new COF-based chemical or biological sensors with better performance and new applications is still far from the end.

Author Contributions: Writing—original draft preparation, G.W. and S.Z.; writing—review and editing, S.Z. and D.L.; project administration, D.L.; funding acquisition, D.L. and G.W. All authors have read and agreed to the published version of the manuscript.

Funding: This work was funded by the National Natural Science Foundation of China, grant number 52172085, 21704023.

Institutional Review Board Statement: Not applicable.

Informed Consent Statement: Not applicable.

Data Availability Statement: No new data were created or analyzed in this study. Data sharing is not applicable to this article.

Acknowledgments: We thank Liangcan He from Harbin Institute of Technology for helpful discussion.

Conflicts of Interest: The authors declare no conflict of interest.

References

1. Diamond, D.; Coyle, S.; Scarmagnani, S.; Hayes, J. Wireless Sensor Networks and Chemo-/Biosensing. *Chem. Rev.* **2008**, *108*, 652–679. [[CrossRef](#)] [[PubMed](#)]
2. Joo, S.; Brown, R.B. Chemical Sensors with Integrated Electronics. *Chem. Rev.* **2008**, *108*, 638–651. [[CrossRef](#)] [[PubMed](#)]
3. Aksyuk, V.A. Sensing without Power. *Nat. Nanotechnol.* **2017**, *12*, 940–941. [[CrossRef](#)] [[PubMed](#)]
4. Lou, Z.; Wang, L.; Shen, G. Recent Advances in Smart Wearable Sensing Systems. *Adv. Mater. Technol.* **2018**, *3*, 1800444. [[CrossRef](#)]
5. Mondal, S.; Zehra, N.; Choudhury, A.; Iyer, P.K. Wearable Sensing Devices for Point of Care Diagnostics. *ACS Appl. Bio Mater.* **2021**, *4*, 47–70. [[CrossRef](#)]
6. Yang, B.; Jiang, X.; Fang, X.; Kong, J. Wearable Chem-biosensing Devices: From Basic Research to Commercial Market. *Lab Chip* **2021**, *21*, 4285–4310. [[CrossRef](#)]
7. Liu, H.; Wang, L.; Lin, G.; Feng, Y. Recent Progress in the Fabrication of Flexible Materials for Wearable Sensors. *Biomater. Sci.* **2022**, *10*, 614–632. [[CrossRef](#)]
8. Liu, Y.; Dong, X.; Chen, P. Biological and Chemical Sensors Based on Graphene Materials. *Chem. Soc. Rev.* **2012**, *41*, 2283–2307. [[CrossRef](#)]
9. Zhao, Y.; Li, X.; Zhou, X.; Zhang, Y. Review on the Graphene Based Optical Fiber Chemical and Biological Sensors. *Sensors Actuat. B-Chem.* **2016**, *231*, 324–340. [[CrossRef](#)]
10. Angizi, S.; Khalaj, M.; Alem, S.A.A.; Pakdel, A.; Willander, M.; Hatamie, A.; Simchi, A. Towards the Two-dimensional Hexagonal Boron Nitride (2D h-BN) Electrochemical Sensing Platforms. *J. Electrochem. Soc.* **2020**, *167*, 126513. [[CrossRef](#)]
11. Gan, X.; Zhao, H.; Quan, X. Two-dimensional MoS₂: A Promising Building Block for Biosensors. *Biosens. Bioelectron.* **2017**, *89*, 56–71. [[CrossRef](#)]
12. Pumera, M.; Loo, A.H. Layered Transition-metal Dichalcogenides (MoS₂ and WS₂) for Sensing and Biosensing. *TrAC-Trend. Anal. Chem.* **2014**, *61*, 49–53. [[CrossRef](#)]
13. Sinha, A.; Dhanjai; Zhao, H.M.; Huang, Y.J.; Lu, X.B.; Chen, J.P.; Jain, R. MXene: An Emerging Material for Sensing and Biosensing. *TrAC-Trend. Anal. Chem.* **2018**, *105*, 424–435. [[CrossRef](#)]
14. Wales, D.J.; Grand, J.; Ting, V.P.; Burke, R.D.; Edler, K.J.; Bowen, C.R.; Mintova, S.; Burrows, A.D. Gas Sensing Using Porous Materials for Automotive Applications. *Chem. Soc. Rev.* **2015**, *44*, 4290–4321. [[CrossRef](#)]
15. Lin, R.-B.; Liu, S.-Y.; Ye, J.-W.; Li, X.-Y.; Zhang, J.-P. Photoluminescent Metal-Organic Frameworks for Gas Sensing. *Adv. Sci.* **2016**, *3*, 1500434. [[CrossRef](#)]
16. Koo, W.T.; Jang, J.S.; Kim, I.D. Metal-Organic Frameworks for Chemiresistive Sensors. *Chem* **2019**, *5*, 1938–1963. [[CrossRef](#)]
17. Teo, W.L.; Liu, J.; Zhou, W.; Zhao, Y. Facile Preparation of Antibacterial MOF-fabric Systems for Functional Protective Wearables. *SmartMat* **2021**, *2*, 567–578. [[CrossRef](#)]
18. Meng, Z.; Mirica, K.A. Covalent Organic Frameworks as Multifunctional Materials for Chemical Detection. *Chem. Soc. Rev.* **2021**, *50*, 13498–13558. [[CrossRef](#)]
19. Liu, X.; Huang, D.; Lai, C.; Zeng, G.; Qin, L.; Wang, H.; Yi, H.; Li, B.; Liu, S.; Zhang, M.; et al. Recent Advances in Covalent Organic Frameworks (COFs) as a Smart Sensing Material. *Chem. Soc. Rev.* **2019**, *48*, 5266. [[CrossRef](#)]
20. Allendorf, M.D.; Dong, R.; Feng, X.; Kaskel, S.; Matoga, D.; Stavila, V. Electronic Devices Using Open Framework Materials. *Chem. Rev.* **2020**, *120*, 8581–8640. [[CrossRef](#)]
21. Geng, K.; He, T.; Liu, R.; Dalapati, S.; Tan, K.; Li, Z.; Tao, S.; Gong, Y.; Jiang, Q.; Jiang, D. Covalent Organic Frameworks: Design, Synthesis, and Functions. *Chem. Rev.* **2020**, *120*, 8814–8933. [[CrossRef](#)]
22. Liu, R.; Tan, K.; Gong, Y.; Chen, Y.; Li, Z.; Xie, S.; He, T.; Lu, Z.; Yang, H.; Jiang, D. Covalent Organic Frameworks: An Ideal Platform for Designing Ordered Materials and Advanced Applications. *Chem. Soc. Rev.* **2021**, *50*, 120–242. [[CrossRef](#)]

23. Jiang, D. Covalent Organic Frameworks: An Amazing Chemistry Platform for Designing Polymers. *Chem* **2020**, *6*, 2461–2483. [[CrossRef](#)]
24. Li, Z.; He, T.; Gong, Y.; Jiang, D. Covalent Organic Frameworks: Pore Design and Interface Engineering. *Acc. Chem. Res.* **2020**, *53*, 1672–1685. [[CrossRef](#)]
25. Li, Y.; Chen, W.; Xing, G.; Jiang, D.; Chen, L. New Synthetic Strategies Towards Covalent Organic Frameworks. *Chem. Soc. Rev.* **2020**, *49*, 2852–2868. [[CrossRef](#)]
26. Jin, P.; Niu, X.; Zhang, F.; Dong, K.; Dai, H.; Zhang, H.; Wang, W.; Chen, H.; Chen, X. Stable and Reusable Light-Responsive Reduced Covalent Organic Framework (COF–300–AR) as an Oxidase-Mimicking Catalyst for GSH Detection in Cell Lysate. *ACS Appl. Mater. Interfaces* **2020**, *12*, 20414–20422. [[CrossRef](#)]
27. Li, G.; Ma, W.; Yang, Y.; Zhong, C.; Huang, H.; Ouyang, D.; He, Y.; Tian, W.; Lin, J.; Lin, Z. Nanoscale Covalent Organic Frameworks with Donor–Acceptor Structures as Highly Efficient Light-Responsive Oxidase-like Mimics for Colorimetric Detection of Glutathione. *ACS Appl. Mater. Interfaces* **2021**, *13*, 49482–49489. [[CrossRef](#)]
28. Xu, M.; Chen, K.; Zhu, L.; Zhang, S.; Wang, M.; He, L.; Zhang, Z.; Du, M. MOF@COF Heterostructure Hybrid for Dual-Mode Photoelectrochemical–Electrochemical HIV-1 DNA Sensing. *Langmuir* **2021**, *37*, 13479–13492. [[CrossRef](#)]
29. Cui, W.-R.; Zhang, C.-R.; Jiang, W.; Liang, R.-P.; Wen, S.-H.; Peng, D.; Qiu, J.-D. Covalent Organic Framework Nanosheet-Based Ultrasensitive and Selective Colorimetric Sensor for Trace Hg²⁺ Detection. *ACS Sustain. Chem. Eng.* **2019**, *7*, 9408–9415. [[CrossRef](#)]
30. Côté, A.P.; Benin, A.I.; Ockwig, N.W.; O’keeffe, M.; Matzger, A.J.; Yaghi, O.M. Porous, Crystalline, Covalent Organic Frameworks. *Science* **2005**, *310*, 1166–1170. [[CrossRef](#)]
31. Furukawa, H.; Yaghi, O.M. Storage of Hydrogen, Methane, and Carbon Dioxide in Highly Porous Covalent Organic Frameworks for Clean Energy Applications. *J. Am. Chem. Soc.* **2009**, *131*, 8875–8883. [[CrossRef](#)] [[PubMed](#)]
32. Tao, S.; Jiang, D. Covalent Organic Frameworks for Energy Conversions: Current Status, Challenges, and Perspectives. *CCS Chem.* **2021**, *3*, 2003–2024. [[CrossRef](#)]
33. Wang, S.; Wang, Q.; Shao, P.; Han, Y.; Gao, X.; Ma, L.; Yuan, S.; Ma, X.; Zhou, J.; Feng, X.; et al. Exfoliation of Covalent Organic Frameworks into Few-Layer Redox-Active Nanosheets as Cathode Materials for Lithium-Ion Batteries. *J. Am. Chem. Soc.* **2017**, *139*, 4258–4261. [[CrossRef](#)] [[PubMed](#)]
34. Han, S.S.; Furukawa, H.; Yaghi, O.M.; Goddard, W.A., III. Covalent Organic Frameworks as Exceptional Hydrogen Storage Materials. *J. Am. Chem. Soc.* **2008**, *130*, 11580–11581. [[CrossRef](#)]
35. Wang, Z.; Zhang, S.; Chen, Y.; Zhang, Z.; Ma, S. Covalent Organic Frameworks for Separation Applications. *Chem. Soc. Rev.* **2020**, *49*, 708–735. [[CrossRef](#)] [[PubMed](#)]
36. Yuan, S.; Li, X.; Zhu, J.; Zhang, G.; Van Puyvelde, P.; Van der Bruggen, B. Covalent Organic Frameworks for Membrane Separation. *Chem. Soc. Rev.* **2019**, *48*, 2665–2681. [[CrossRef](#)] [[PubMed](#)]
37. Liang, Z.; Wang, H.-Y.; Zheng, H.; Zhang, W.; Cao, R. Porphyrin-based Frameworks for Oxygen Electrocatalysis and Catalytic Reduction of Carbon Dioxide. *Chem. Soc. Rev.* **2021**, *50*, 2540–2581. [[CrossRef](#)] [[PubMed](#)]
38. Sharma, R.K.; Yadav, P.; Yadav, M.; Gupta, R.; Rana, P.; Srivastava, A.; Zbořil, R.; Varma, R.S.; Antonietti, M.; Gawande, M.B. Recent Development of Covalent Organic Frameworks (COFs): Synthesis and Catalytic (Organic-Electro-Photo) Applications. *Mater. Horiz.* **2020**, *7*, 411–454. [[CrossRef](#)]
39. Liu, J.G.; Wang, N.; Ma, L.L. Recent Advances in Covalent Organic Frameworks for Catalysis. *Chem-Asian J.* **2020**, *15*, 338–351. [[CrossRef](#)]
40. Yusran, Y.; Li, H.; Guan, X.; Fang, Q.; Qiu, S. Covalent Organic Frameworks for Catalysis. *EnergyChem* **2020**, *2*, 100035. [[CrossRef](#)]
41. Ren, X.; Li, C.; Kang, W.; Li, H.; Ta, N.; Ye, S.; Hu, L.; Wang, X.; Li, C.; Yang, Q. Enormous Promotion of Photocatalytic Activity through the Use of Near-Single Layer Covalent Organic Frameworks. *CCS Chem.* **2021**, *3*, 2453–2463. [[CrossRef](#)]
42. Ding, S.-Y.; Dong, M.; Wang, Y.-W.; Chen, Y.-T.; Wang, H.-Z.; Su, C.-Y.; Wang, W. Thioether-Based Fluorescent Covalent Organic Framework for Selective Detection and Facile Removal of Mercury(II). *J. Am. Chem. Soc.* **2016**, *138*, 3031–3037. [[CrossRef](#)]
43. Wang, J.; Zhuang, S. Covalent Organic Frameworks (COFs) for Environmental Applications. *Coord. Chem. Rev.* **2019**, *400*, 213046. [[CrossRef](#)]
44. Li, C.; Liu, L.; Kang, J.; Xiao, Y.; Feng, Y.; Cao, F.-F.; Zhang, H. Pristine MOF and COF Materials for Advanced Batteries. *Energy Stor. Mater.* **2020**, *31*, 115–134. [[CrossRef](#)]
45. Feng, L.; Qian, C.; Zhao, Y. Recent Advances in Covalent Organic Framework-Based Nanosystems for Bioimaging and Therapeutic Applications. *ACS Mater. Lett.* **2020**, *2*, 1074–1092. [[CrossRef](#)]
46. Bhambri, H.; Khullar, S.; Sakshi; Mandal, S.K. Nitrogen-rich Covalent Organic Frameworks: A Promising Class of Sensory Materials. *Mater. Adv.* **2022**, *3*, 19–124. [[CrossRef](#)]
47. Ascherl, L.; Evans, E.W.; Gorman, J.; Orsborne, S.; Bessinger, D.; Bein, T.; Friend, R.H.; Auras, F. Perylene-Based Covalent Organic Frameworks for Acid Vapor Sensing. *J. Am. Chem. Soc.* **2019**, *141*, 15693–15699. [[CrossRef](#)]
48. EL-Mahdy, A.F.M.; Laia, M.-Y.; Kuo, S.-W. A Highly Fluorescent Covalent Organic Framework as A Hydrogen Chloride Sensor: Roles of Schiff Base Bonding and π -Stacking. *J. Mater. Chem. C* **2020**, *8*, 9520–9528. [[CrossRef](#)]
49. Wang, M.; Hu, M.; Liu, J.; Guo, C.; Peng, D.; Jia, Q.; He, L.; Zhang, Z.; Du, M. Covalent Organic Framework-based ElectroChemical Aptasensors for the Ultrasensitive Detection of Antibiotics. *Biosens. Bioelectron.* **2019**, *132*, 8–16. [[CrossRef](#)]

50. Xiong, Y.; Su, L.; He, X.; Duan, Z.; Zhang, Z.; Chen, Z.; Xie, W.; Zhu, D.; Luo, Y. Colorimetric Determination of Copper Ions Based on Regulation of the Enzyme-Mimicking Activity of Covalent Triazine Frameworks. *Sens. Actuators B* **2017**, *253*, 384–391. [[CrossRef](#)]
51. Skorjanc, T.; Shetty, D.; Valant, M. Covalent Organic Polymers and Frameworks for Fluorescence-Based Sensors. *ACS Sens.* **2021**, *6*, 1461–1481. [[CrossRef](#)]
52. Guo, L.; Yang, L.; Li, M.; Kuang, L.; Song, Y.; Wang, L. Covalent Organic Frameworks for Fluorescent Sensing: Recent Developments and Future Challenges. *Coord. Chem. Rev.* **2021**, *440*, 213957. [[CrossRef](#)]
53. Ascherl, L.; Evans, E.W.; Hennemann, M.; Nuzzo, D.D.; Hufnagel, A.G.; Beetz, M.; Friend, R.H.; Clark, T.; Bein, T.; Auras, F. Solvatochromic Covalent Organic Frameworks. *Nat. Commun.* **2018**, *9*, 3802. [[CrossRef](#)]
54. Huang, W.; Jiang, Y.; Li, X.; Li, X.; Wang, J.; Wu, Q.; Liu, X. Solvothermal Synthesis of Microporous, Crystalline Covalent Organic Framework Nanofibers and Their Colorimetric Nanohybrid Structures. *ACS Appl. Mater. Interfaces* **2013**, *5*, 8845–8849. [[CrossRef](#)]
55. Jhulki, S.; Evans, A.M.; Hao, X.L.; Cooper, M.W.; Feriante, C.H.; Leisen, J.; Li, H.; Lam, D.; Hersam, M.C.; Barlow, S.; et al. Humidity Sensing through Reversible Isomerization of a Covalent Organic Framework. *J. Am. Chem. Soc.* **2020**, *142*, 783–791. [[CrossRef](#)]
56. Singh, H.; Tomer, V.K.; Jena, N.; Bala, I.; Sharma, N.; Nepak, D.; Sarkar, A.D.; Kailasam, K.; Pal, S.K. A Porous, Crystalline Truxene-Based Covalent Organic Framework and Its Application in Humidity Sensing. *J. Mater. Chem. A* **2017**, *5*, 21820–21827. [[CrossRef](#)]
57. Kulkarni, R.; Noda, Y.; Barange, D.K.; Kochergin, Y.S.; Lyu, P.; Balcarova, B.; Nachtigall, P.; Bojdys, M.J. Real-Time Optical and Electronic Sensing with a β -Amino Enone Linked, Triazine-Containing 2D Covalent Organic Framework. *Nat. Commun.* **2019**, *10*, 3228. [[CrossRef](#)]
58. Yuan, H.; Li, N.; Linghu, J.; Dong, J.; Wang, Y.; Karmakar, A.; Yuan, J.; Li, M.; Buenconsejo, P.J.S.; Liu, G.; et al. Chip-Level Integration of Covalent Organic Frameworks for Trace Benzene Sensing. *ACS Sens.* **2020**, *5*, 1474–1481. [[CrossRef](#)]
59. Doonan, C.J.; Tranchemontagne, D.J.; Glover, T.G.; Hunt, J.R.; Yaghi, O.M. Exceptional Ammonia Uptake by a Covalent Organic Framework. *Nat. Chem.* **2010**, *2*, 235–238. [[CrossRef](#)] [[PubMed](#)]
60. Dalapati, S.; Jin, E.; Addicoat, M.; Heine, T.; Jiang, D. Highly Emissive Covalent Organic Frameworks. *J. Am. Chem. Soc.* **2016**, *138*, 5797–5800. [[CrossRef](#)] [[PubMed](#)]
61. Sharma, N.; Sharma, N.; Srinivasan, P.; Kumar, S.; Rayappan, J.B.B.; Kailasam, K. Heptazine Based Organic Framework as a Chemiresistive Sensor for Ammonia Detection at Room Temperature. *J. Mater. Chem. A* **2018**, *6*, 18389–18395. [[CrossRef](#)]
62. Xu, N.; Wang, R.-L.; Li, D.-P.; Zhou, Z.-Y.; Zhang, T.; Xie, Y.-Z.; Su, Z.-M. Continuous Detection of HCl and NH₃ Gases with a High-Performance Fluorescent Polymer Sensor. *New J. Chem.* **2018**, *42*, 13367–13374. [[CrossRef](#)]
63. Yang, Y.; Zhao, Z.; Yan, Y.; Li, G.; Hao, C. A Mechanism of the Luminescent Covalent Organic Framework for the Detection of NH₃. *New J. Chem.* **2019**, *43*, 9274–9279. [[CrossRef](#)]
64. Meng, Z.; Stolz, R.M.; Mirica, K.A. Two-Dimensional Chemiresistive Covalent Organic Framework with High Intrinsic Conductivity. *J. Am. Chem. Soc.* **2019**, *141*, 11929–11937. [[CrossRef](#)]
65. Niu, F.; Shao, Z.-W.; Zhu, J.-L.; Tao, L.-M.; Ding, Y. Structural Evolution of Imine-linked Covalent Organic Frameworks and Their NH₃ Sensing Performance. *J. Mater. Chem. C* **2021**, *9*, 8562–8569. [[CrossRef](#)]
66. Cui, F.-Z.; Xie, J.-J.; Jiang, S.-Y.; Gan, S.-X.; Ma, D.-L.; Liang, R.-R.; Jiang, G.-F.; Zhao, X. A Gaseous Hydrogen Chloride Chemosensor Based on a 2D Covalent Organic Framework. *Chem. Commun.* **2019**, *55*, 4550–4553. [[CrossRef](#)]
67. Gilmanova, L.; Bon, V.; Shupletsov, L.; Pohl, D.; Rauche, M.; Brunner, E.; Kaskel, S. Chemically Stable Carbazole-Based Imine Covalent Organic Frameworks with Acidochromic Response for Humidity Control Applications. *J. Am. Chem. Soc.* **2021**, *143*, 18368–18373. [[CrossRef](#)]
68. Ko, W.C.; Kim, M.-S.; Kwon, Y.J.; Jeong, J.; Kim, W.R.; Choi, H.; Park, J.K.; Jeong, Y.K. Two-Dimensional Semiconducting Covalent Organic Nanosheets for Highly Sensitive and Stable NO₂ Sensing Under Humid Conditions. *J. Mater. Chem. A* **2020**, *8*, 19246–19253. [[CrossRef](#)]
69. Yang, K.; Yuan, W.; Hua, Z.; Tang, Y.; Yin, F.; Xia, D. Triazine-Based Two-Dimensional Organic Polymer for Selective NO₂ Sensing with Excellent Performance. *ACS Appl. Mater. Interfaces* **2020**, *12*, 3919–3927. [[CrossRef](#)]
70. Yue, Y.; Cai, P.; Xu, X.; Li, H.; Chen, H.; Zhou, H.-C.; Huang, N. Conductive Metallophthalocyanine Framework Films with High Carrier Mobility as Efficient Chemiresistors. *Angew. Chem. Int. Ed.* **2021**, *60*, 10806–10813. [[CrossRef](#)]
71. Guo, L.; Wang, M.; Zeng, X.; Cao, D. Luminescent Porous Organic Polymer Nanotubes for Highly Selective Sensing of H₂S. *Mater. Chem. Front.* **2017**, *1*, 2643–2650.
72. Yan, D.; Wang, Z.; Cheng, P.; Chen, Y.; Zhang, Z. Rational Fabrication of Crystalline Smart Materials for Rapid Detection and Efficient Removal of Ozone. *Angew. Chem. Int. Ed.* **2021**, *60*, 6055–6060. [[CrossRef](#)] [[PubMed](#)]
73. Cui, W.-R.; Jiang, W.; Zhang, C.-R.; Liang, R.-P.; Liu, J.; Qiu, J.-D. Regenerable Carbohydrazide-Linked Fluorescent Covalent Organic Frameworks for Ultrasensitive Detection and Removal of Mercury. *ACS Sustain. Chem. Eng.* **2020**, *8*, 445–451. [[CrossRef](#)]
74. Yin, Y.; Liu, G. Application of Synthesized 2,5-bis(allyloxy)terephthalohydrazide Functionalized Covalent Organic Framework Material as a Fluorescence Probe for Selective Detection of Mercury (II). *Mater. Today Commun.* **2021**, *27*, 102440. [[CrossRef](#)]
75. Li, Z.; Zhang, Y.; Xi, H.; Mu, Y.; Liu, X. A Robust and Luminescent Covalent Organic Framework as A Highly Sensitive and Selective Sensor for the Detection of Cu²⁺ Ions. *Chem. Commun.* **2016**, *52*, 6613–6616. [[CrossRef](#)]

76. Cui, Y.; Liu, Y.; Liu, J.; Du, J.; Yu, Y.; Wang, S.; Liang, Z.; Yu, J. Multifunctional Porous Tröger's Base Polymers with Tetraphenylethene Units: CO₂ Adsorption, Luminescence and Sensing Properties. *Polym. Chem.* **2017**, *8*, 4842–4848. [[CrossRef](#)]
77. Jin, E.; Li, J.; Geng, K.; Jiang, Q.; Xu, H.; Xu, Q.; Jiang, D. Designed Synthesis of Stable Light-Emitting Two-Dimensional sp² Carbon-Conjugated Covalent Organic Frameworks. *Nat. Commun.* **2018**, *9*, 4143. [[CrossRef](#)]
78. Cai, Y.; Jiang, Y.; Feng, L.; Hua, Y.; Liu, H.; Fan, C.; Yin, M.; Li, S.; Lv, X.; Wang, H. Q-graphene-scaffolded Covalent Organic Frameworks as Fluorescent Probes and Sorbents for the Fluorimetry and Removal of Copper Ions. *Anal. Chim. Acta* **2019**, *1057*, 88–97. [[CrossRef](#)]
79. Wang, T.; Xue, R.; Chen, H.; Shi, P.; Lei, X.; Wei, Y.; Guo, H.; Yang, W. Preparation of Two New Polyimide Bond Linked Porous Covalent Organic Frameworks and Their Fluorescence Sensing Application for Sensitive and Selective Determination of Fe³⁺. *New J. Chem.* **2017**, *41*, 14272–14278. [[CrossRef](#)]
80. Li, M.; Cui, Z.; Pang, S.; Meng, L.; Ma, D.; Li, Y.; Shi, Z.; Feng, S. Luminescent Covalent Organic Framework as a Recyclable Turn-off Fluorescent Sensor for Cations and Anions in Aqueous Solution. *J. Mater. Chem. C* **2019**, *7*, 11919–11925. [[CrossRef](#)]
81. Wu, X.; Wang, B.; Yang, Z.; Chen, L. Novel Imine-linked Covalent Organic Frameworks: Preparation, Characterization and Application. *J. Mater. Chem. A* **2019**, *7*, 5650–5655. [[CrossRef](#)]
82. Chen, G.; Lan, H.-H.; Cai, S.-L.; Sun, B.; Li, X.-L.; He, Z.-H.; Zheng, S.-R.; Fan, J.; Liu, Y.; Zhang, W.-G. Stable Hydrazone-Linked Covalent Organic Frameworks Containing O,N,O'-Chelating Sites for Fe(III) Detection in Water. *ACS Appl. Mater. Interfaces* **2019**, *11*, 12830–12837. [[CrossRef](#)]
83. Cui, D.; Ding, X.; Xie, W.; Xu, G.; Su, Z.; Xu, Y.; Xie, Y. A Tetraphenylethylene-based Covalent Organic Framework for Waste Gas Adsorption and Highly Selective Detection of Fe³⁺. *CrystEngComm* **2021**, *23*, 5569–5574. [[CrossRef](#)]
84. Li, D.-M.; Zhang, S.-Y.; Wan, J.-Y.; Zhang, W.-Q.; Yan, Y.-L.; Tang, X.-H.; Zheng, S.-R.; Cai, S.-L.; Zhang, W.-G. A New Hydrazone-linked Covalent Organic Framework for Fe(III) Detection by Fluorescence and QCM Technologies. *CrystEngComm* **2021**, *23*, 3594–3601. [[CrossRef](#)]
85. Liang, X.; Ni, Z.; Zhao, L.; Ge, B.; Zhao, H.; Li, W. Multifunctional Triphenylbenzene-based Polyimide Covalent Organic Framework with Absolute Eclipsed Stacking Models for Fluorescence Detecting of Fe³⁺ and Electrochemical Detecting of Pb²⁺. *Microchem. J.* **2021**, *170*, 106663. [[CrossRef](#)]
86. Zhang, T.; Gao, C.; Huang, W.; Chen, Y.; Wang, Y.; Wang, J. Covalent Organic Framework as A Novel Electrochemical Platform for Highly Sensitive and Stable Detection of Lead. *Talanta* **2018**, *188*, 578–583. [[CrossRef](#)]
87. Wang, R.; Ji, W.; Huang, L.; Guo, L.; Wang, X. Electrochemical Determination of Lead(II) in Environmental Waters Using a Sulfhydryl Modified Covalent Organic Framework by Square Wave Anodic Stripping Voltammetry (SWASV). *Anal. Lett.* **2019**, *52*, 1757–1770. [[CrossRef](#)]
88. Zhao, C.; Zhang, L.; Wang, Q.; Zhang, L.; Zhu, P.; Yu, J.; Zhang, Y. Porphyrin-Based Covalent Organic Framework Thin Films as Cathodic Materials for “On–Off–On” Photoelectrochemical Sensing of Lead Ions. *ACS Appl. Mater. Interfaces* **2021**, *13*, 20397–20404. [[CrossRef](#)]
89. Zhou, Z.; Zhong, W.; Cui, K.; Zhuang, Z.; Li, L.; Li, L.; Bi, J.; Yu, Y. A Covalent Organic Framework Bearing Thioether Pendant Arms for Selective Detection and Recovery of Au from Ultra-low Concentration Aqueous Solution. *Chem. Commun.* **2018**, *54*, 9977–9980. [[CrossRef](#)]
90. Cui, W.-R.; Zhang, C.-R.; Jiang, W.; Li, F.-F.; Liang, R.-P.; Liu, J.; Qiu, J.-D. Regenerable and Stable sp² Carbon-conjugated Covalent Organic Frameworks for Selective Detection and Extraction of Uranium. *Nat. Commun.* **2020**, *11*, 436. [[CrossRef](#)]
91. Zhang, L.; Yang, G.-P.; Xiao, S.-J.; Tan, Q.-G.; Zheng, Q.-Q.; Liang, R.-P.; Qiu, J.-D. Facile Construction of Covalent Organic Framework Nanozyme for Colorimetric Detection of Uranium. *Small* **2021**, *17*, 2102944. [[CrossRef](#)]
92. Chen, Y.; Sun, R.; Zhu, W.; Zhang, Z.; Chen, Y.; Wang, S.; Deng, Q. Desirability of Position 2, 2'-bipyridine Group into COFs for the Fluorescence Sensing of Ni(II). *Sens. Actuators B Chem.* **2021**, *344*, 130216. [[CrossRef](#)]
93. Zhang, S.; Chen, K.; Zhu, L.; Xu, M.; Song, Y.; Zhang, Z.; Du, M. Direct Growth of Two-dimensional Phthalocyanine-based COF on Cu-MOF to Construct a Photoelectrochemical-Electrochemical Dual-mode Biosensing Platform for High-efficiency Determination of Cr(III). *Dalton Trans.* **2021**, *50*, 14285–14295. [[CrossRef](#)]
94. Lu, Y.; Liang, Y.; Zhao, Y.; Xia, M.; Liu, X.; Shen, T.; Feng, L.; Yuan, N.; Chen, Q. Fluorescent Test Paper via the In Situ Growth of COFs for Rapid and Convenient Detection of Pd(II) Ions. *ACS Appl. Mater. Interfaces* **2021**, *13*, 1644–1650. [[CrossRef](#)]
95. Yue, J.-Y.; Ding, X.-L.; Wang, Y.-T.; Wen, Y.-X.; Yang, P.; Ma, Y.; Tang, B. Dual Functional sp² Carbon-conjugated Covalent Organic Frameworks for Fluorescence Sensing and Effective Removal and Recovery of Pd²⁺ Ions. *J. Mater. Chem. A* **2021**, *9*, 26861–26866. [[CrossRef](#)]
96. Wang, Z.; Meng, Q.; Ma, R.; Wang, Z.; Yang, Y.; Sha, H.; Ma, X.; Ruan, X.; Zou, X.; Yuan, Y.; et al. Constructing an Ion Pathway for Uranium Extraction from Seawater. *Chem* **2020**, *6*, 1683–1691. [[CrossRef](#)]
97. Yuan, Y.; Yang, Y.; Ma, X.; Meng, Q.; Wang, L.; Zhao, S.; Zhu, G. Molecularly Imprinted Porous Aromatic Frameworks and Their Composite Components for Selective Extraction of Uranium Ions. *Adv. Mater.* **2018**, *30*, 1706507. [[CrossRef](#)]
98. Li, Z.; Meng, Q.; Yang, Y.; Zou, X.; Yuan, Y.; Zhu, G. Constructing Amidoxime-modified Porous Adsorbents with Open Architecture for Cost-effective and Efficient Uranium Extraction. *Chem. Sci.* **2020**, *11*, 4747–4752. [[CrossRef](#)]
99. Cui, W.-R.; Li, F.; Xu, R.-H.; Zhang, C.-R.; Chen, X.-R.; Yan, R.-H.; Liang, R.-P.; Qiu, J.-D. Regenerable Covalent Organic Frameworks for Photo-enhanced Uranium Adsorption from Seawater. *Angew. Chem. Int. Ed.* **2020**, *59*, 17684–17690. [[CrossRef](#)] [[PubMed](#)]

100. Zhang, Y.; Shen, X.; Feng, X.; Xia, H.; Mu, Y.; Liu, X. Covalent Organic Frameworks as pH Responsive Signaling Scaffolds. *Chem. Commun.* **2016**, *52*, 11088–11091. [[CrossRef](#)]
101. Chen, L.; He, L.; Ma, F.; Liu, W.; Wang, Y.; Silver, M.A.; Chen, L.; Zhu, L.; Gui, D.; Diwu, J.; et al. Covalent Organic Framework Functionalized with 8-Hydroxyquinoline as a Dual-Mode Fluorescent and Colorimetric pH Sensor. *ACS Appl. Mater. Interfaces* **2018**, *10*, 15364–15368. [[CrossRef](#)] [[PubMed](#)]
102. Xu, M.; Wang, L.; Xie, Y.; Song, Y.; Wang, L. Ratiometric Electrochemical Sensing and Biosensing Based on Multiple Redox-Active State COFDHTA-TTA. *Sens. Actuators B Chem.* **2019**, *281*, 1009–1015. [[CrossRef](#)]
103. Yuan, F.; Kong, Y.; You, J.; Zhang, C.; Xian, Y. Rational Synthesis of Imine-Linked Fluorescent Covalent Organic Frameworks with Different pK_a for pH Sensing In Vitro and In Vivo. *ACS Appl. Mater. Interfaces* **2021**, *13*, 51351–51361. [[CrossRef](#)] [[PubMed](#)]
104. Chen, Z.; Wang, K.; Hu, X.; Shi, P.; Guo, Z.; Zhan, H. Novel One-Dimensional Covalent Organic Framework as a H⁺ Fluorescent Sensor in Acidic Aqueous Solution. *ACS Appl. Mater. Interfaces* **2021**, *13*, 1145–1151. [[CrossRef](#)]
105. Li, Z.; Li, H.; Xia, H.; Ding, X.; Luo, X.; Liu, X.; Mu, Y. Triarylboron-Linked Conjugated Microporous Polymers: Sensing and Removal of Fluoride Ions. *Chem. Eur. J.* **2015**, *21*, 17355–17362. [[CrossRef](#)]
106. Li, Z.; Huang, N.; Lee, K.H.; Feng, Y.; Tao, S.; Jiang, Q.; Nagao, Y.; Irlle, S.; Jiang, D. Light-Emitting Covalent Organic Frameworks: Fluorescence Improving via Pinpoint Surgery and Selective Switch-On Sensing of Anions. *J. Am. Chem. Soc.* **2018**, *140*, 12374–12377. [[CrossRef](#)]
107. Su, L.; Zhang, Z.; Xiong, Y. Water Dispersed Two-dimensional Ultrathin Fe(III)-Modified Covalent Triazine Framework Nanosheets: Peroxidase Like Activity and Colorimetric Biosensing Applications. *Nanoscale* **2018**, *10*, 20120–20125. [[CrossRef](#)]
108. Wang, P.; Zhou, F.; Zhang, C.; Yin, S.-Y.; Teng, L.; Chen, L.; Hu, X.-X.; Liu, H.-W.; Yin, X.; Zhang, X.-B. Ultrathin Two-dimensional Covalent Organic Framework Nanoprobe for Interference-Resistant Two-Photon Fluorescence Bioimaging. *Chem. Sci.* **2018**, *9*, 8402–8408. [[CrossRef](#)]
109. Paul, B.D.; Snyder, S.H. H₂S Signalling Through Protein Sulphydration and Beyond. *Nat. Rev. Mol. Cell Biol.* **2012**, *13*, 499–507. [[CrossRef](#)]
110. Gadalla, M.M.; Snyder, S.H. Hydrogen sulfide as a gasotransmitter. *J. Neurochem.* **2010**, *113*, 14–26. [[CrossRef](#)]
111. Zhang, W.; Qiu, L.-G.; Yuan, Y.-P.; Xie, A.-J.; Shen, Y.-H.; Zhu, J.-F. Microwave-assisted Synthesis of Highly Fluorescent Nanoparticles of a Melamine-based Porous Covalent Organic Framework for Trace-level Detection of Nitroaromatic Explosives. *J. Hazard. Matter.* **2012**, *221–222*, 147–154. [[CrossRef](#)]
112. Sang, N.; Zhan, C.; Cao, D. Highly Sensitive and Selective Detection of 2,4,6-trinitrophenol Using Covalent-Organic Polymer Luminescent Probes. *J. Mater. Chem. A* **2015**, *3*, 92–96. [[CrossRef](#)]
113. Guo, L.; Cao, D.; Yun, J.; Zeng, X. Highly Selective Detection of Picric Acid from Multicomponent Mixtures of Nitro Explosives by Using COP Luminescent Probe. *Sens. Actuators B Chem.* **2017**, *243*, 753–760. [[CrossRef](#)]
114. Jiang, S.; Meng, L.; Ma, W.; Qia, Q.; Zhang, W.; Xua, B.; Liu, L.; Tian, W. Morphology Controllable Conjugated Network Polymers Based on AIE-active Building Block for TNP Detection. *Chin. Chem. Lett.* **2021**, *32*, 1037–1040. [[CrossRef](#)]
115. Rao, M.R.; Fang, Y.; Feyter, S.D.; Perepichka, D.F. Conjugated Covalent Organic Frameworks via Michael Addition-Elimination. *J. Am. Chem. Soc.* **2017**, *139*, 2421–2427. [[CrossRef](#)]
116. Dalapati, S.; Jin, S.; Gao, J.; Xu, Y.; Nagai, A.; Jiang, D. An Azine-Linked Covalent Organic Framework. *J. Am. Chem. Soc.* **2013**, *135*, 17310–17313. [[CrossRef](#)]
117. Xiang, Z.; Cao, D. Synthesis of Luminescent Covalent–Organic Polymers for Detecting Nitroaromatic Explosives and Small Organic Molecules. *Macromol. Rapid Commun.* **2012**, *33*, 1184–1190. [[CrossRef](#)]
118. Kaleeswaran, D.; Vishnoi, P.; Murugavel, R. [3+3] Imine and β-ketoenamine Tethered Fluorescent Covalent-Organic Frameworks for CO₂ Uptake and Nitroaromatic Sensing. *J. Mater. Chem. C* **2015**, *3*, 7159–7171. [[CrossRef](#)]
119. Das, G.; Biswal, B.P.; Kandambeth, S.; Venkatesh, V.; Kaur, G.; Addicoat, M.; Heine, T.; Verma, S.; Banerjee, R. Chemical Sensing in Two Dimensional Porous Covalent Organic Nanosheets. *Chem. Sci.* **2015**, *6*, 3931–3939. [[CrossRef](#)]
120. Gomes, R.; Bhaumik, A. A New Triazine Functionalized Luminescent Covalent Organic Framework for Nitroaromatic Sensing and CO₂ Storage. *RSC Adv.* **2016**, *6*, 28047–28054. [[CrossRef](#)]
121. Lin, G.; Ding, H.; Yuan, D.; Wang, B.; Wang, C. A Pyrene-Based, Fluorescent Three-Dimensional Covalent Organic Framework. *J. Am. Chem. Soc.* **2016**, *138*, 3302–3305. [[CrossRef](#)] [[PubMed](#)]
122. Zhang, C.; Zhang, S.; Yan, Y.; Xia, F.; Huang, A.; Xian, Y. Highly Fluorescent Polyimide Covalent Organic Nanosheets as Sensing Probes for the Detection of 2,4,6-Trinitrophenol. *ACS Appl. Mater. Interfaces* **2017**, *9*, 13415–13421. [[CrossRef](#)] [[PubMed](#)]
123. Kaleeswaran, D.; Murugavel, R. Picric Acid Sensing and CO₂ Capture by a Sterically Encumbered Azo-linked Fluorescent Triphenylbenzene Based Covalent Organic Polymer. *J. Chem. Sci.* **2018**, *130*, 1. [[CrossRef](#)]
124. Das, P.; Mandal, S.K. A Dual-functionalized, Luminescent and Highly Crystalline Covalent Organic Framework: Molecular Decoding Strategies for VOCs and Ultrafast TNP Sensing. *J. Mater. Chem. A* **2018**, *6*, 16246–16256. [[CrossRef](#)]
125. Wang, S.; Liu, Y.; Yu, Y.; Du, J.; Cui, Y.; Song, X.; Liang, Z. Conjugated Microporous Polymers Based on Biphenylene for CO₂ Adsorption and Luminescence Detection of Nitroaromatic Compounds. *New J. Chem.* **2018**, *42*, 9482–9487. [[CrossRef](#)]
126. Gao, Q.; Li, X.; Ning, G.-H.; Leng, K.; Tian, B.; Liu, C.; Tang, W.; Xu, H.-S.; Loh, K.P. Highly Photoluminescent Two-dimensional Iminebased Covalent Organic Frameworks for Chemical Sensing. *Chem. Commun.* **2018**, *54*, 2349–2352. [[CrossRef](#)]
127. Faheem, M.; Aziz, S.; Jing, X.; Ma, T.; Du, J.; Sun, F.; Tian, Y.; Zhu, G. Dual Luminescent Covalent Organic Frameworks for Nitro-explosive Detection. *J. Mater. Chem. A* **2019**, *7*, 27148–27155. [[CrossRef](#)]

128. Pan, L.; Liu, Z.; Tian, M.; Schroeder, B.C.; Aliev, A.E.; Faul, C.F.J. Luminescent and Swellable Conjugated Microporous Polymers for Detecting Nitroaromatic Explosives and Removing Harmful Organic Vapors. *ACS Appl. Mater. Interfaces* **2019**, *11*, 48352–48362. [[CrossRef](#)]
129. Das, P.; Chakraborty, G.; Mandal, S.K. Comprehensive Structural and Microscopic Characterization of an Azine–Triazine-Functionalized Highly Crystalline Covalent Organic Framework and Its Selective Detection of Dichloran and 4-Nitroaniline. *ACS Appl. Mater. Interfaces* **2020**, *12*, 10224–10232. [[CrossRef](#)]
130. Chen, J.-Q.; Zheng, Q.-Q.; Xiao, S.-J.; Zhang, L.; Liang, R.-P.; Ouyang, G.; Qiu, J.-D. Construction of Two-Dimensional Fluorescent Covalent Organic Framework Nanosheets for the Detection and Removal of Nitrophenols. *Anal. Chem.* **2022**, *94*, 2517–2526. [[CrossRef](#)]
131. Zhao, Y.; Liu, X.; Li, Y.; Xia, M.; Xia, T.; Sun, H.; Sui, Z.; Hu, X.-M.; Chen, Q. Ultra-Stable Fluorescent 2D Covalent Organic Framework for Rapid Adsorption and Selective Detection of Radioiodine. *Microporous Mesoporous Mater.* **2021**, *319*, 111046. [[CrossRef](#)]
132. Wang, P.; Xu, Q.; Li, Z.; Jiang, W.; Jiang, Q.; Jiang, D. Exceptional Iodine Capture in 2D Covalent Organic Frameworks. *Adv. Mater.* **2018**, *30*, 1801991. [[CrossRef](#)]
133. Geng, T.; Zhang, W.; Zhu, Z.; Kai, X. Triazine-based conjugated microporous polymers constructing triphenylamine and its derivatives with nitrogen as core for iodine adsorption and fluorescence sensing I₂. *Microporous Mesoporous Mater.* **2019**, *273*, 163–170. [[CrossRef](#)]
134. Geng, T.; Ma, L.; Chen, G.; Zhang, C.; Zhang, W.; Xia, H.; Zhu, H. Poly[1,3,6,8-tetra(2-thiophenyl)pyrene] and poly[1,3,6,8-tetra(3-thiophenyl)pyrene] conjugated microporous polymers for reversible adsorbing and fluorescent sensing iodine. *J. Polym. Res.* **2019**, *26*, 113. [[CrossRef](#)]
135. Geng, T.; Liu, M.; Zhang, C.; Hu, C.; Xu, H. Synthesis of secondary amine-based fluorescent porous organic polymers via Friedel–Crafts polymerization reaction for adsorbing and fluorescent sensing iodine. *J. Appl. Polym. Sci.* **2020**, *137*, e49255. [[CrossRef](#)]
136. Geng, T.; Zhang, C.; Chen, G.; Ma, L.; Zhang, W.; Xia, H. Synthesis of tetraphenylethylene-based fluorescent conjugated microporous polymers for fluorescent sensing and adsorbing iodine. *Microporous Mesoporous Mater.* **2019**, *284*, 468–475. [[CrossRef](#)]
137. Geng, T.; Chen, G.; Ma, L.; Zhang, C.; Zhang, W.; Xu, H. The spirobifluorene-based fluorescent conjugated microporous polymers for reversible adsorbing iodine, fluorescent sensing iodine and nitroaromatic compounds. *Eur. Polym. J.* **2019**, *115*, 37–44. [[CrossRef](#)]
138. Geng, T.; Ma, L.; Chen, G.; Zhang, C.; Zhang, W.; Niu, Q. Fluorescent conjugated microporous polymers containing pyrazine moieties for adsorbing and fluorescent sensing of iodine. *Environ. Sci. Pollut. Res.* **2020**, *27*, 20235–20245. [[CrossRef](#)]
139. Geng, T.; Zhang, C.; Hu, C.; Liu, M.; Fei, Y.; Xia, H. Synthesis of 1,6-disubstituted pyrene-based conjugated microporous polymers for reversible adsorption and fluorescence sensing of iodine. *New J. Chem.* **2020**, *44*, 2312–2320. [[CrossRef](#)]
140. Zhang, T.; Chen, Y.; Huang, W.; Wang, Y.; Hu, X. A Novel AuNPs–doped COFs Composite as Electrochemical Probe for Chlorogenic Acid Detection with Enhanced Sensitivity and Stability. *Sens. Actuators B Chem.* **2018**, *276*, 362–369. [[CrossRef](#)]
141. Wang, Y.; Wang, Y.; Liu, H. A Novel Fluorescence and SPE Adsorption Nanomaterials of Molecularly Imprinted Polymers Based on Quantum Dot-Grafted Covalent Organic Frameworks for the High Selectivity and Sensitivity Detection of Ferulic Acid. *Nanomaterials* **2019**, *9*, 305. [[CrossRef](#)]
142. Sun, Y.; Xua, L.; Waterhouse, G.I.N.; Wang, M.; Qiao, X.; Xu, Z. Novel Three-dimensional Electrochemical Sensor with Dual Signal Amplification Based on MoS₂ Nanosheets and High-conductive NH₂MWCNT@COF for Sulfamerazine Determination. *Sens. Actuators B Chem.* **2019**, *281*, 107–114. [[CrossRef](#)]
143. Zhou, N.; Ma, Y.; Hu, B.; He, L.; Wang, S.; Zhang, Z.; Lu, S. Construction of Ce–MOF@COF Hybrid Nanostructure: Label-free Aptasensor for the Ultrasensitive Detection of Oxytetracycline Residues in Aqueous Solution Environments. *Biosens. Bioelectron.* **2019**, *127*, 92–100. [[CrossRef](#)]
144. Ma, X.; Pang, C.; Li, S.; Xiong, Y.; Li, J.; Luo, J.; Yang, Y. Synthesis of Zr-coordinated Amide Porphyrin-based Two-dimensional Covalent Organic Framework at Liquid-liquid Interface for Electrochemical Sensing of Tetracycline. *Biosens. Bioelectron.* **2019**, *146*, 111734. [[CrossRef](#)]
145. Wang, J.-M.; Lian, X.; Yan, B. Eu³⁺-Functionalized Covalent Organic Framework Hybrid Material as a Sensitive Turn-On Fluorescent Switch for Levofloxacin Monitoring in Serum and Urine. *Inorg. Chem.* **2019**, *58*, 9956–9963. [[CrossRef](#)]
146. Zhang, D.; Liu, H.; Geng, W.; Wang, Y. A Dual-function Molecularly Imprinted Optopolymer Based on Quantum Dots-grafted Covalent-Organic Frameworks for the Sensitive Detection of Tyramine in Fermented Meat Products. *Food Chem.* **2019**, *277*, 639–645. [[CrossRef](#)]
147. Dong, J.; Li, X.; Peh, S.B.; Yuan, Y.D.; Wang, Y.; Ji, D.; Peng, S.; Liu, G.; Ying, S.; Yuan, D.; et al. Restriction of Molecular Rotors in Ultrathin Two-Dimensional Covalent Organic Framework Nanosheets for Sensing Signal Amplification. *Chem. Mater.* **2019**, *31*, 146–160. [[CrossRef](#)]
148. Gua, Y.; Wang, J.; Shia, H.; Pana, M.; Liu, B.; Fang, G.; Wang, S. Electrochemiluminescence sensor based on upconversion nanoparticles and oligoaniline-crosslinked gold nanoparticles imprinting recognition sites for the determination of dopamine. *Biosens. Bioelectron.* **2019**, *128*, 129–136. [[CrossRef](#)]
149. Yao, X.; Shen, J.; Liu, Q.; Fa, H.; Yang, M.; Hou, C. A Novel Electrochemical Aptasensor for the Sensitive Detection of Kanamycin Based on UiO-66NH₂/MCA/MWCNT@rGONR Nanocomposites. *Anal. Methods* **2020**, *12*, 4967–4976. [[CrossRef](#)]

150. Wang, J.; Zhao, L.; Yan, B. Indicator Displacement Assay Inside Dye-Functionalized Covalent Organic Frameworks for Ultrasensitive Monitoring of Sialic Acid, an Ovarian Cancer Biomarker. *ACS Appl. Mater. Interfaces* **2020**, *12*, 12990–12997. [[CrossRef](#)]
151. Han, Z.-Y.; Zhang, H.; Li, H.-K.; Zhu, Q.-Q.; He, H. Ingenious Construction of an Electrochemical Aptasensor based on a Au@COF/GO–NH₂ Composite with Excellent Detection Performance. *J. Mater. Chem. C* **2021**, *9*, 4576. [[CrossRef](#)]
152. Yang, M.; Mao, Y.; Wang, B.; Lin, L.; Wang, Y.; Zhang, L.; Jiang, Y.; Zhao, M.; Chen, H.; Zhang, Y. Heterometallic Mg@Fe–MIL–101/TpPa–1–COF Grown on Stainless Steel Mesh: Enhancing Photo-degradation, Fluorescent Detection and Toxicity Assessment for Tetracycline Hydrochloride. *Colloid Surf. A* **2021**, *631*, 127725. [[CrossRef](#)]
153. Zhao, N.; Liu, J.; Yang, F.; Lv, S.; Wang, J.; Wang, S. Easy Green Construction of a Universal Sensing Platform Based on Crystalline Polyimide Covalent Organic Frameworks with Sensitive Fluorescence Response to Metal Ions and Antibiotics. *ACS Appl. Bio Mater.* **2021**, *4*, 995–1002. [[CrossRef](#)]
154. Wang, J.; Qu, X.; Zhao, L.; Yan, B. Fabricating Nanosheets and Ratiometric Detection of 5-Fluorouracil by Covalent Organic Framework Hybrid Material. *Anal. Chem.* **2021**, *93*, 4308–4316. [[CrossRef](#)]
155. Song, Y.; Ma, R.; Hao, L.; Yang, X.; Wang, C.; Wu, Q.; Wang, Z. Application of Covalent Organic Framework as the Adsorbent for Solid-phase Extraction of Trace Levels of Pesticide Residues Prior to High-performance Liquid Chromatography-Ultraviolet Detection. *J. Chromatogr. A* **2018**, *1572*, 20–26. [[CrossRef](#)]
156. Ji, W.-H.; Guo, Y.-S.; Wang, X.; Lu, X.-F.; Guo, D.-S. Amino-modified Covalent Organic Framework as Solid Phase Extraction Absorbent for Determination of Carboxylic Acid Pesticides in Environmental Water Samples. *J. Chromatogr. A* **2019**, *1595*, 11–18. [[CrossRef](#)]
157. Liu, H.; Zhang, Y.; Zhang, D.; Zheng, F.; Huang, M.; Sun, J.; Sun, X.; Li, H.; Wang, J.; Sun, B. A Fluorescent Nanoprobe for 4-ethylguaiaicol Based on the Use of A Molecularly Imprinted Polymer Doped with A Covalent Organic Framework Grafted onto Carbon Nanodots. *Microchim. Acta* **2019**, *186*, 182. [[CrossRef](#)]
158. Kandambeth, S.; Mallick, A.; Lukose, B.; Mane, M.V.; Heine, T.; Banerjee, R. Construction of Crystalline 2D Covalent Organic Frameworks with Remarkable Chemical (Acid/Base) Stability via a Combined Reversible and Irreversible Route. *J. Am. Chem. Soc.* **2012**, *134*, 19524–19527. [[CrossRef](#)]
159. Liu, X.; Chen, H.; Wang, R.; Zang, S.-Q.; Mak, T.C.W. Cationic Covalent-Organic Framework as Efficient Redox Motor for High-Performance Lithium–Sulfur Batteries. *Small* **2020**, *16*, 2002932. [[CrossRef](#)]
160. Wang, J.; Yang, X.; Wei, T.; Bao, J.; Zhu, Q.; Dai, Z. Fe-Porphyrin-Based Covalent Organic Framework As a Novel Peroxidase Mimic for a One-Pot Glucose Colorimetric Assay. *ACS Appl. Bio Mater.* **2018**, *1*, 382–388. [[CrossRef](#)]
161. Zhao, Y.; Xu, X.; Ma, Y.; Tan, H.; Li, Y. A novel Peroxidase/oxidase Mimetic Fe-porphyrin Covalent Organic Framework Enhanced the Luminol Chemiluminescence Reaction and Its Application in Glucose Sensing. *Luminescence* **2020**, *35*, 1366–1372. [[CrossRef](#)]
162. Yue, J.-Y.; Ding, X.-L.; Wang, L.; Yang, R.; Bi, J.-S.; Song, Y.-W.; Yang, P.; Ma, Y.; Tang, B. Novel Enzyme-Functionalized Covalent Organic Frameworks for the Colorimetric Sensing of Glucose in Body Fluids and Drinks. *Mater. Chem. Front.* **2021**, *5*, 3859–3866. [[CrossRef](#)]
163. He, Y.; Lin, X.; Tang, Y.; Ye, L. A Selective Sensing Platform for the Simultaneous Detection of Ascorbic acid, Dopamine, and Uric Acid Based on AuNPs/carboxylated COFs/Poly(fuchsin basic) Film. *Anal. Methods* **2021**, *13*, 4503–4514. [[CrossRef](#)]
164. Wu, X.; Han, X.; Xu, Q.; Liu, Y.; Yuan, C.; Yang, S.; Liu, Y.; Jiang, J.; Cui, Y. Chiral BINOL-Based Covalent Organic Frameworks for Enantioselective Sensing. *J. Am. Chem. Soc.* **2019**, *141*, 7081–7089. [[CrossRef](#)]
165. Zhang, T.; Ma, N.; Ali, A.; Wei, Q.; Wu, D.; Ren, X. Electrochemical Ultrasensitive Detection of Cardiac Troponin I Using Covalent Organic Frameworks for Signal Amplification. *Biosens. Bioelectron.* **2018**, *119*, 176–181. [[CrossRef](#)]
166. Feng, S.; Yan, M.; Xue, Y.; Huang, J.; Yang, X. Electrochemical Immunosensor for Cardiac Troponin I Detection Based on Covalent Organic Framework and Enzyme-Catalyzed Signal Amplification. *Anal. Chem.* **2021**, *93*, 13572–13579. [[CrossRef](#)]
167. Zhai, R.; Gong, X.Y.; Xie, J.; Yuan, Y.; Xu, F.; Jiang, Y.; Huang, Z.; Dai, X.; Zhang, Y.; Qian, X.; et al. Ultrasensitive Analysis of Heat Shock Protein 90α with Antibodies Orderly Arrayed on a Novel Type of Immunoprobe Based on Magnetic COFs. *Talanta* **2019**, *191*, 553–560. [[CrossRef](#)]
168. Ma, Y.; Lu, M.; Deng, Y.; Bai, R.; Zhang, X.; Li, D.; Zhang, K.; Hu, R.; Yang, Y. The Preparation of C-Reactive Protein Immunosensor Based on Nano-Mimetic Enzyme Co₃O₄. *J. Biomed. Nanotechnol.* **2018**, *14*, 1169–1177. [[CrossRef](#)]
169. Deng, Y.; Du, X.; Ma, Y.; Zhang, K.; Zhang, X.; Li, D.-L.; Bai, R.; Hu, R.; Yang, Y.-H. Development of C-Reactive Protein Immunosensor Using Thionine/Au Nanoparticles-Covalent Organic Framework-LZU8 as Label. *Nanosci. Nanotechnol. Lett.* **2018**, *10*, 520–527. [[CrossRef](#)]
170. Liu, T.-Z.; Hu, R.; Zhang, X.; Zhang, K.-L.; Liu, Y.; Zhang, X.-B.; Bai, R.-Y.; Li, D.; Yang, Y.-H. Metal–Organic Framework Nanomaterials as Novel Signal Probes for Electron Transfer Mediated Ultrasensitive Electrochemical Immunoassay. *Anal. Chem.* **2016**, *88*, 12516–12523. [[CrossRef](#)]
171. Li, W.; Yang, C.-X.; Yan, X.-P. A Versatile Covalent Organic Framework-based Platform for Sensing Biomolecules. *Chem. Commun.* **2017**, *53*, 11469–11471. [[CrossRef](#)]
172. Peng, Y.; Huang, Y.; Zhu, Y.; Chen, B.; Wang, L.; Lai, Z.; Zhang, Z.; Zhao, M.; Tan, C.; Yang, N.; et al. Ultrathin Two-Dimensional Covalent Organic Framework Nanosheets: Preparation and Application in Highly Sensitive and Selective DNA Detection. *J. Am. Chem. Soc.* **2017**, *139*, 8698–8704. [[CrossRef](#)]

173. Mal, A.; Mishra, R.K.; Praveen, V.K.; Khayum, M.A.; Banerjee, R.; Ajayaghosh, A. Supramolecular Reassembly of Self-Exfoliated Ionic Covalent Organic Nanosheets for Label-Free Detection of Double-Stranded DNA. *Angew. Chem. Int. Ed.* **2018**, *57*, 8443–8447. [[CrossRef](#)] [[PubMed](#)]
174. Zhang, X.; Chi, K.-N.; Li, D.-L.; Deng, Y.; Ma, Y.-C.; Xu, Q.-Q.; Hu, R.; Yang, Y.-H. 2D-porphrinic Covalent Organic Framework-Based Aptasensor with Enhanced Photoelectrochemical Response for the Detection of C-reactive Protein. *Biosens. Bioelectron.* **2019**, *129*, 64–71. [[CrossRef](#)]